2009

Estimating the Degree of Space Weathering on Koronis Family Asteroids Using ECAS

Andrea Domokos

Estimating the Degree of Space Weathering on Koronis Family Asteroids Using ECAS

(Spine title: Characterization of Space Weathering Using an ECAS System)

(Thesis format: Monograph)

by

Andrea Domokos

Graduate Program in Physics
Department of Physics and Astronomy

A thesis submitted in partial fulfillment of the requirements for the degree of Master of Science

School of Graduate and Postdoctoral Studies
The University of Western Ontario
London, Ontario, Canada

Abstract

Space weathering processes are those which act to modify the spectral properties of airless bodies like asteroids. Hiroi et al. [*LPSC XXXVI*, abstract no. 1396, 2006] recently suggested a new method for estimating the degree of weathering on a body's surface using an Eight Colour Asteroid Survey (ECAS) type filter system. From May to September 2007, a series of ground-based telescopic observations of Koronis family asteroids in four ECAS colors was carried out to test this method; this study represents the first thorough analysis of Hiroi et al.'s method to date. The results presented here include analysis of the dozen Koronis asteroids observed by the author as well as the data given in Zellner et al. (1985) [Icarus 61, 355-416] for other S-type asteroids in the Main Belt. The spectral properties found are shown, in general, to be consistent with previous studies using other photometric systems. However, while the ECAS inflection method for estimating the degree of space weathering on asteroid surfaces has potential, it was found to be very challenging to obtain reliable results for bodies in space.

Keywords: asteroids, asteroid surfaces minor planets, photometry, regoliths, solar system, spectroscopy

Acknowledgements

I'd like to thank my supervisor, Dr. Paul Wiegert, for taking a chance on this project and letting me run with it. Without his support, encouragement, guidance, and infinite patience, it would not have seen the light of day.

David Balam, at The University of Victoria, provided a wealth of helpful advice when it came to observing. From taking the perfect flats to the ins and outs of IRAF, Dave always made himself available to provide assistance wherever it was necessary. I owe whatever talent for observing I have developed to his wisdom. Dave's assistance with the photometric calibrations is also much appreciated.

There are several other individuals without whom this project would not have been possible: I thank Dr. David Gray and Mike Debruyne for the use of the Elginfield observatory and their support as I learned my way around the instruments; Dmitry Monin at the Dominion Astrophysical Observatory for his tireless efforts to accommodate all of my observing requirements; Dr. Peter Brown of the UWO Meteor Physics Group for his advice as the project got underway, the ECAS filters, and for giving me my start in Planetary Science research; and the members of the UWO Meteor Physics Group with whom I've spent my days for the last several years, I thank them for their support and their wonderful senses of humour that kept me sane.

Finally, a big thanks to my family for their constant encouragement, their forgiveness of my absences when the office or observatory become my second home, and their patience during the many times when it felt like this would never end.

Contents

List of Figures

List of Tables

List of Abbreviations

AU	Astronomical Unit
CCD	Charged-Coupled Device
DAO	Dominion Astrophysical Observatory
ECAS	Eight Colour Asteroid Survey
IRAF	Image Reduction and Analysis Facility
NEA	Near-Earth asteroid
OC	Ordinary chondrite
SDSS	Sloan Digital Sky Survey
SMASSII	Small Main-Belt Asteroid Spectroscopic Survey, Phase II
SMFe	Sub-microscopic Iron

Chapter 1

Introduction

1.1 Asteroids

1.1.1 Overview

Planet formation in the inner solar system began with the accumulation of dust from the solar nebula into kilometre-sized planetesimals. The largest planetesimals continued to accrete, through gravitational attraction, into larger protoplanets which ultimately formed the terrestrial planets. Asteroids are planetesimals that were never able to accrete into larger, planet-sized bodies. They are found throughout the solar system, though most are located in the Main Belt, between the orbits of Mars and Jupiter. Gravitational perturbations, mostly from Jupiter, have disrupted the Main Belt population (Fig. 1.1), leading to collisions that formed the asteroid families and caused the ejection of Main Belt asteroids into the inner solar system. The Near Earth Asteroids (NEAs) are asteroids that have been "kicked out" of the Main Belt and now reside, at least part of the time, inside of Mars' orbit. Some NEAs also cross Earth's orbit. Other asteroid groups include the Trojan population - those which orbit at the Lagrange points of certain planets. Mars has five Trojans, Neptune has two, and Jupiter has a cluster of Trojans at its L_4 and L_5 Lagrange points, leading and trailing its orbit by 60°. To date, over 400,000 asteroids have identified orbits[1].

[1] Minor Planet Centre Archive Statistics: http://www.cfa.harvard.edu/iau/lists/ArchiveStatistics.html

Within the different asteroid populations there is significant variation in structure and composition. Most asteroids are believed to be "rubble-piles", made up of fragments and debris from the collisional break-up of larger bodies which have since reaccumulated (Britt and Consolmagno 2001). At least one, (4) Vesta, is known to be differentiated and it is believed that there are many more differentiated bodies yet to be identified in the Main Belt (Moskovitz et al. 2008). Evidence suggests that compositions vary from silicate and metal-rich bodies in the inner solar system to organic-rich asteroids farther from the sun (Gradie and Tedesco 1982).

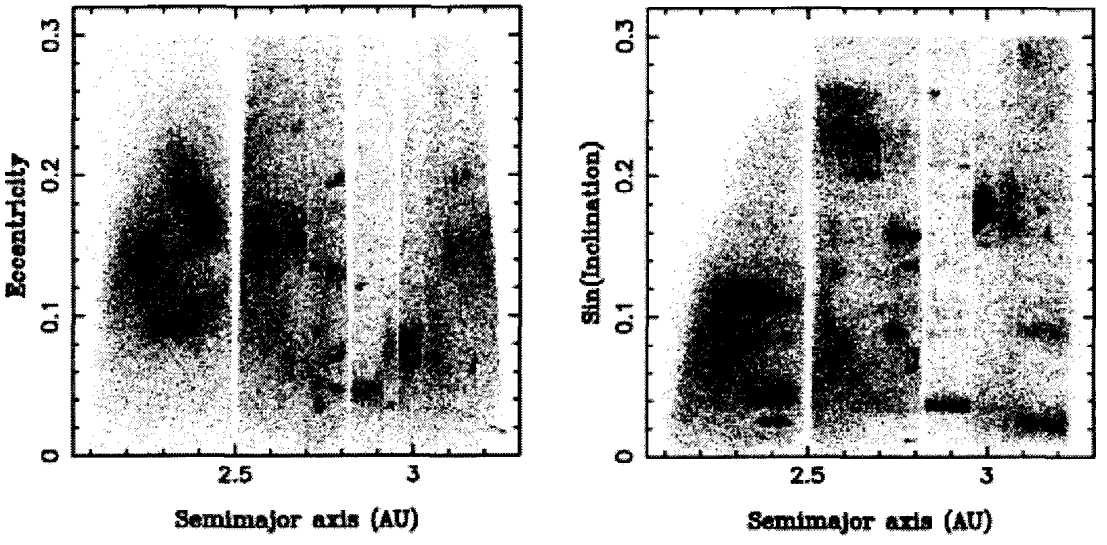

Figure 1.1: Distribution of Main Belt asteroids in orbital element space. The dark clusters represent asteroid families. The gaps (Kirkwood gaps) are regions that have been cleared by resonances with Jupiter (Nesvorný et al. 2005b).

1.1.2 Observation and Classification

Detailed information about the rotational properties and composition of individual bodies is usually obtained via remote sensing methods such as light curve photometry and reflectance spectroscopy. All asteroids are airless bodies, so incident

sunlight is scattered or absorbed by mineral grains on their surfaces. The fraction of light that is reflected toward Earth varies with wavelength, depending on the optical properties of those grains; this gives asteroids their "colour" (Bus et al. 2002). When asteroids are observed with CCD (charged-coupled device) imagers, their colours can be measured through different photometric filters ("photometry"). The changes in colour with time can be used to generate light curves, which are plots of the asteroid's brightness as a function of time that allow rotational characteristics like period, shape, and spin axis orientation to be determined (e.g. Slivan et al. 1996). Spectroscopy, on the other hand, is most useful for making inferences about the composition of the bodies.

The fraction of light that is reflected from the asteroid at a given wavelength is the reflectance and a spectrum is the variation of reflectance with wavelength. For asteroids, the reflectance between 0.35 – 3.2 μm (visible – near infrared) is studied most often since this is where particulate minerals at the surface produce absorption bands in the spectra. Each major mineral has a characteristic band location, so the absorption bands can be diagnostic of surface composition and are used to make inferences about the bulk mineral composition (Clark et al. 2002; Bus et al. 2002). Note that this technique can only indicate the minerals which may be present at the surface; it does not allow for a direct determination of the bulk composition, so there is always a degree of uncertainty when making such inferences.

Direct observations of asteroids (as opposed to remote sensing) are much less common but there have been several spacecraft flybys and a few dedicated missions: Near-Earth Asteroid Rendezvous (NEAR) Shoemaker visited asteroids (253)

Mathilde and (433) Eros, actually landing on the latter's surface (see Izenberg et al. 2003 for results of spectroscopic analysis on Eros). The Galileo spacecraft provided flyby images of (951) Gaspra and (423) Ida on its way to Jupiter (c.f. Chapman 1996). Those images contained the first colour evidence for space weathering on asteroids and will be discussed in further detail in Chapter 2. The Japanese Space Agency's Hayabusa spacecraft visited (25143) Itokawa and was intended to be the first sample-return mission. It left Itokawa in April of 2007 and is expected to arrive back at Earth in 2010[2]. Finally, NASA/JPL's Dawn mission was launched in September 2007 and is on its way to investigate (4) Vesta and (1) Ceres. While these missions have provided valuable data, direct observing with spacecraft is very costly and time consuming, so remote sensing remains the primary means of obtaining useful information about asteroids.

Both spectroscopy and photometry have been used to classify asteroids according to their colours and inferred mineralogies. The most commonly used classification schemes are the Tholen taxonomy, based on photometric data obtained during the Eight Colour Asteroid Survey (ECAS) (Tholen 1984; Zellner et al. 1985b), and the Small Main-Belt Asteroid Spectroscopic Survey, Phase II (SMASSII) taxonomy, based on spectral features (Bus and Binzel 2002). Combined, these schemes define three major classes, or complexes, of asteroids: S, C, and X (note that the X complex in the SMASSII system corresponds to the E, M, and P classes in the Tholen system. See Bus et al. 2002 for detailed description of taxonomies and the characteristics of each spectral class). The S complex, made up of silicate-rich bodies, dominates the near Earth environment and the inner Main

[2] JAXA ISAS: http://www.isas.ac.jp/e/enterp/missions/hayabusa/index.shtml

Belt. In fact, 80% of NEAs with known taxonomic types belong to this class (Bottke et al. 2002). The central belt is dominated by the C complex, which are the dark, carbonaceous bodies. The D-types and the P-types (the latter belonging to the X complex) are concentrated in the outer belt and in the Trojan populations.

1.1.3 Asteroid Families

Asteroid families are formed when a large asteroid is catastrophically disrupted, usually through a collision, leaving behind smaller fragments that are clustered in proper orbital element space, i.e. proper semimajor axis, proper inclination, and proper eccentricity. Unlike the instantaneous, or osculating elements, proper a, i, and e are quantities that remain constant over time and are thus a more reliable means of defining an object's original location in phase space. Because family members share a common origin, they are compositionally similar and can be distinguished from the background population by spectral shape or colour (Ivezić et al. 2002; Nesvorný et al. 2005). This makes them particularly useful for studying the collisional evolution of bodies, and better understanding their internal structure and the physical processes that may modify them over time. Dynamical modeling of asteroid families allows for age estimates, so the ages of many families are now known (Nesvorný et al. 2005b). The dynamical ages represent the time since the disruption from which they formed.

The Koronis family, used in this study, formed from the collisional disruption of a single parent body ~2.5 Gy ago and contains the Karin cluster, a young sub-family formed ~5.8 My ago (Nesvorný et al. 2005b). Koronis is one of

the three major asteroid families and, like the others, has its own distinct colour type (Ivezić et al. 2002). There are ~2300 known members, of which 31 have full spectral classification. The majority of its members are S-types and are spectrally homogenous (Mothé-Diniz et al. 2005).

1.1.4 Associations with Meteorites

Meteorites are the portions of rocky debris that have survived the fall through Earth's atmosphere. Since meteorites represent the most primitive material available to us in the solar system, studying meteorites has been a way to learn about solar system formation and evolution processes within a lab environment. For meteorite analysis to be truly meaningful, however, we need to know where the material originated. Asteroids are generally believed to be the meteorite parent bodies, so it would be useful to know how well meteorites sample the asteroid belt. The first asteroid to be associated with a group of meteorites was (4) Vesta, when it was discovered that its reflectance spectrum was very similar to the spectra of some HED meteorites (Howardites, Eucrites, Diogenites) (McCord et al. 1970). After the Vesta-HED association was made, it was expected that simple spectral matching would yield more asteroid parent bodies for other meteorite groups, particularly for the ordinary chondrites, or OCs.

Ordinary chondrites are the most common in meteorite collections and because the S-class asteroids are the most abundant in the asteroid belt, it was believed that the S-class asteroids are the source of OC meteorites. No S asteroids were found to have spectra matching those of OC meteorites, however, leading to a

paradox now known as the "S-type Conundrum" (Chapman 2004). The spectra of S-type asteroids are generally darker and redder than those of OC meteorite samples. Other asteroid spectral types have been proposed as potential meteorite parent bodies (Scott 2002) but to date, spectral features have not been similar enough to conclusively link them.

The S-type paradox eventually led to the discovery that asteroid spectra could be modified by various processes acting on the surfaces of asteroids, such as ion irradiation by the solar wind. Similar changes were observed during the Apollo missions when comparing lunar rock samples to lunar soils (Colonel and Nash 1970). The modification of optical properties, or space weathering, has often been invoked to explain the discrepancies between asteroid and meteorite spectra.

1.2 The Problem of Space Weathering

Space weathering is formally defined as processes occurring on the surfaces of airless bodies which act to modify their optical properties in a way that can confuse the interpretation of remotely obtained spectra (Hapke 2001; Chapman 2004). The accepted model for space weathering is Hapke's vapour deposition model, in which the optical effects of weathering are caused by the build-up of sub-microscopic iron (SMFe) on the surface regolith particles. The SMFe comes from solar wind sputtering and hypervelocity micrometeorite impacts. The sputtered and vapourized material, primarily Fe-bearing silicate vapours, gets injected downward into the regolith and coats the grains in its path. As more grains are coated with SMFe, the grains become darker and light passing through the particles is reddened.

Consequently, spectra of surfaces that have been weathered are typically darkened and reddened, and characteristic absorption bands are weakened (Fig. 1.2). Lab experiments have shown that small amounts of SMFe can result in significant changes to the optical properties of regolith (loose rock fragments and soil on the surface); the addition of just 0.5% SMFe to a pulverized lunar rock sample can alter its spectrum to resemble that of lunar soil (Hapke 2001). In comparison, 0.025% SMFe can alter a powdered OC meteorite spectrum to look like that of an S-type asteroid (Hapke 2001).

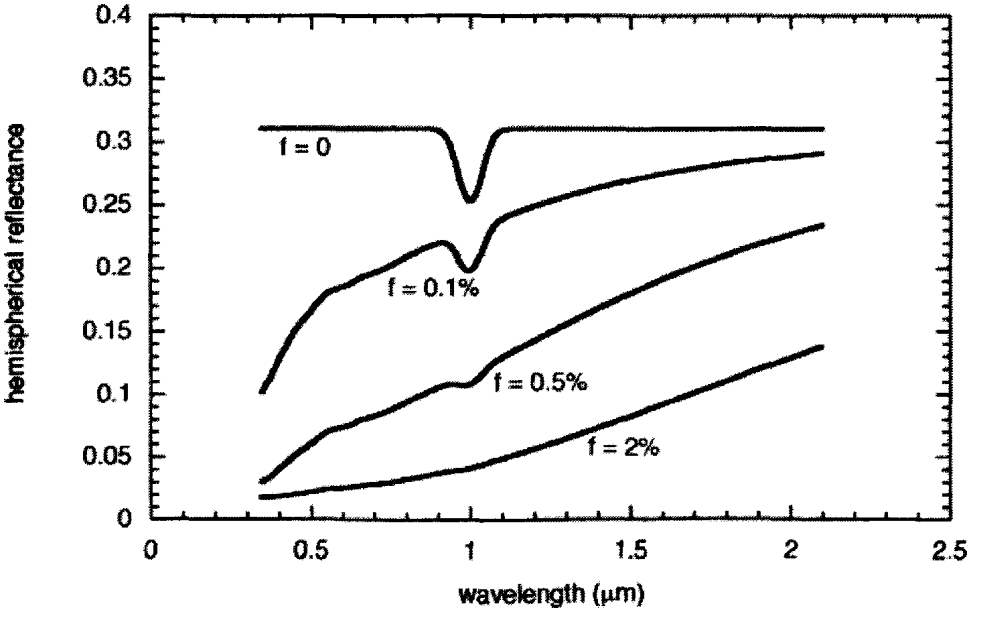

Figure 1.2: Hapke (2001) to demonstrated spectral modification by space weathering using a mathematical model. As the fraction of SMFe is increased, the spectrum becomes redder and the absorption band is weakened.

Space weathering appears to be most effective on surfaces already containing an abundance of Fe, such as the olivine-rich S-class asteroids. Pyroxene-rich surfaces, like those of (4) Vesta and the "Vestoids" are iron-poor and do not respond

as readily to modification by weathering (Clark et al. 2002). Other important factors governing the degree to which a surface will be weathered include the impact energies of micrometeorites, the age of the surface, and the body's ability to retain regolith (Bottke et al. 2002).

As noted in section 1.1.2, remote sensing techniques can only identify minerals present at the surface and we rely on that information to infer the bulk composition of the body. A direct consequence of space weathering is a high uncertainty when making such inferences. The moon, for instance, was thought to be made of OC material until the Surveyor landers returned *in situ* data revealing the lunar surface to be basaltic (Chapman 2004). Weathering also limits our ability to make conclusive associations between meteorite classes and their possible asteroidal parent bodies. The implications of space weathering effects, then, are significant; understanding the link between asteroids and meteorites will allow researchers to study asteroids in the lab, a goal that cannot be fully realized until space weathering is understood.

While the mechanisms for weathering are generally well understood in principle, it has proven challenging to estimate weathering rates. In the lab, irradiation experiments have been used to infer timescales for the dominant processes (e.g. Hapke 2001; Sasaki et al. 2001). Remotely obtained spectra have also been used to characterize weathering, typically with colour plots using band ratios. However, as Hiroi et al. (2006) have pointed out, the usual spectroscopic methods are susceptible to variations in grain size and viewing geometry. It is possible, for

example, for a meteorite sample to appear up to 2.5 times brighter than an asteroid due to the phase angles at which the targets are observed (Clark et al. 2002).

To remedy this, Hiroi et al. (2006) suggest a new method for estimating the degree of weathering on a body that is unaffected by the issues which plague standard methods. Hiroi et al. (2006) focus on inflections in the reflectance curves at 0.42 and 0.55 μm, which they associate with space weathering. They propose that as the degree of space weathering at the surface progresses, negative inflections at these wavelengths will tend towards zero, or become smoother, and that the magnitude of the inflections can be measured using an Eight Colour Asteroid Survey (ECAS) type filter system (Fig. 1.3). Hiroi et al. (2006) irradiated powdered meteorite samples to test this and were successful in demonstrating their expected trends. Their lab results also indicate that this method is not affected by grain size or phase angle up to 60°. To date, their method has not been rigorously tested outside of a lab environment.

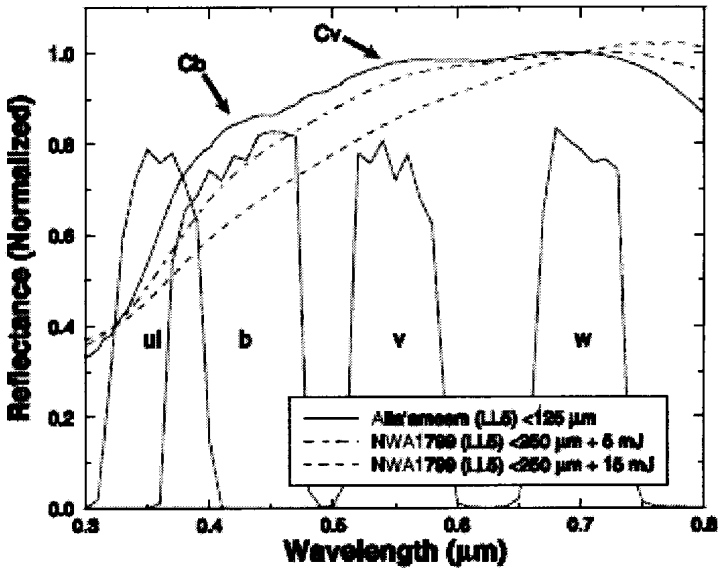

Figure 1.3: Results of Hiroi et al.'s (2006) simulations. The reflectance curve of an unmodified meteorite sample is shown by the solid line and the locations of the C_b and C_v inflections (the "bumps" in the curve) are indicated. The dashed curves represent meteorite samples irradiated by a pulsed laser. As the amount of laser energy to which the samples are subjected is increased, the curves become smoother and steeper; the inflections disappear. The ECAS u, b, v, and w bands are also indicated (Hiroi et al. 2006).

1.3 Thesis Focus

This work aims to test the ideas proposed by Hiroi et al. (2006) through a series of ground-based, photometric observations with an ECAS system. A survey of Koronis Family asteroids in four ECAS colours, as well as the results of the first ECAS survey carried out in the early 1980s (Zellner et al. 1985b) are used to address the following key questions:

1. How effectively can this new method be applied to targets in space?
2. Can the Koronis Family results be extended to a broader population?
3. Can this method allow us to put any new constraints on weathering time scales?

In the following chapter, a detailed overview of the current state of understanding of space weathering on asteroid surfaces, particularly for the S-complex asteroids, will be presented. Chapter 3 describes the target selection process and observations. In Chapter 4, an overview of the all-sky photometry method and the results for each asteroid are given. Chapter 5 presents an analysis of the results for both the Koronis Family observations and the Zellner et al. (1985b) datasets. Finally, Chapter 6 summarizes the key findings, discusses their implications, and suggests further work that may be done to improve these results.

Chapter 2

Literature Review

2.1 The Lunar Model and its Extension to the Asteroid Belt

The idea that the optical properties of a body's surface could be modified was first proposed by Gold in 1955, who theorized that some kind of darkening process may be acting on the lunar surface (Gold 1955). Gold's ideas were confirmed during the Apollo era in the 1970s, when the spectra of freshly pulverized lunar rocks did not match that of lunar soil samples. Compared to the rock samples, the regolith had lower albedo, a redder spectral slope, and the absorption bands near 1 μm and 2 μm were weakened (Fig. 2.1).

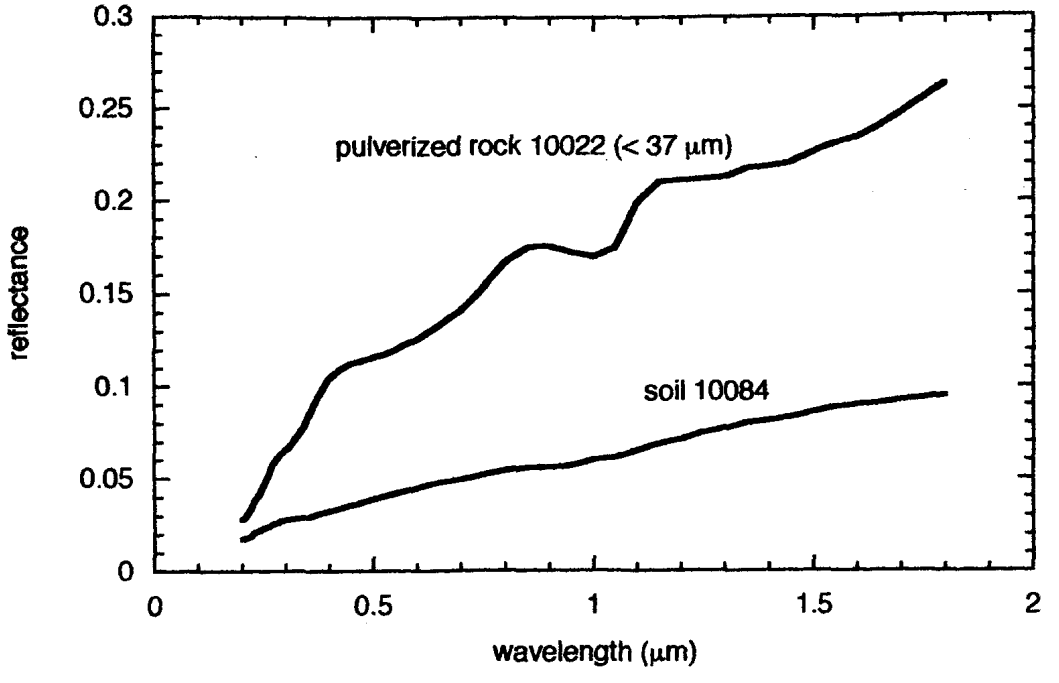

Figure 2.1: Bidirectional reflectance spectra of an Apollo 11 lunar soil (or regolith) sample and lunar rock pulverized to < 37 μm (Hapke 2001).

The spectral modification of surface regolith was initially attributed to impact vitrification by micrometeorite bombardment. According to the vitrification model, hypervelocity impacts at the surface would melt the rocky minerals in the upper layers of the regolith and turn them into glass. Weathering could then be detected by the presence of impact glass, or agglutinates, within the surface regolith. Early lab experiments showed that such a process could lead to the spectral changes observed in lunar samples: powdered rock spectra were darkened and absorption bands were weakened (e.g. Colonel and Nash 1970; Adams and McCord 1971). This model led to the assumption that weathering would not operate in the asteroid belt because impact velocities are too low for agglutinization to occur (McKay et al. 1989). The successful association of (4) Vesta with HED meteorites was seen to validate that assumption, since the spectra were so similar. Also, the lack of agglutinates detected in meteorite samples lead to the conclusion that no agglutinates were present in asteroid regoliths and therefore space weathering did not operate on asteroids (Pieters et al. 2000).

As a consequence of having lunar samples available for analysis, lunar space weathering could be directly characterized and the lunar models served as the basis for our understanding of asteroid weathering. The vitrification model remained the dominant paradigm until the 1990s and because it implied that asteroid surfaces were not subject to significant weathering processes, weathering in the Main Belt was not seriously studied until a new consensus was reached.

An alternative model, the vapor deposition model outlined in Chapter 1, was proposed by Hapke in 1975, who argued that while agglutinization did occur, it was

not likely to be responsible for the modifications seen by remote sensing techniques (Hapke et al. 1975; Hapke 2001). He conducted several experiments showing that earlier vitrification simulations were deeply flawed and did not actually cause any significant spectral modification. According to Hapke (2001), the space weathering model begins with the lunar maturation model of McKay et al. (1974, 1989), which considers the surface regolith to be the product of pulverization by meteorite impact. The impacts break up the rocks and minerals at the surface into smaller particles, which can subsequently be welded together into larger particles by shock vitrification and agglutinization. Hapke's space weathering model holds that in addition to comminution and vitrification, surface regolith is also subjected to hydrogen ions from the solar wind and hypervelocity micrometeorites, processes which can erode and/or vapourize the grains. The sputtered and vapourized material moves downward into the soil, coating the surrounding grains in its path (Hapke 2001). The vapourized material consists mainly of Fe-bearing silicates, which are intrinsically reducing when they condense, resulting in the production of submicroscopic iron (SMFe[3]) coatings on the soil particles (Hapke 2001). Hapke argued that it was these SMFe coatings that were responsible for the spectral modifications seen in lunar soil samples, not agglutinates. He also conducted several experiments to demonstrate that the vapour deposition model does successfully reproduce those changes (summarized in Hapke 2001).

[3] This was initially known as "npFe^0", or nanophase reduced iron, to emphasize the scale and nature of the particles involved (Clark et al. 2002). However, Hapke (2001) showed that a significant amount of the Fe in lunar soil is actually in the > 100 nm range and "SMFe" was adopted by many authors as a more accurate term. Both forms are still used in the literature.

The Hapke model was largely ignored until an experiment by Keller and McKay (1993) provided the first visual proof of the coatings predicted by Hapke's model (Fig. 2.2a). Keller and McKay showed that SMFe was present in vapour-deposited grain coatings (as opposed to melt glass) in lunar soil samples and that, from a remote sensing perspective, those coatings are crucial for the effects seen on spectra because the opaque grains inhibit the multiple scattering and reflection that would otherwise enhance spectral contrast (Chapman 2004). Despite the appearance of these particles in lunar samples, however, lab simulations of lunar-like space weathering failed to reproduce or detect them until an experiment by Sasaki et al. (2001). Using pulsed laser irradiation of olivine samples to simulate high-velocity dust impact, Sasaki et al. (2001) observed SMFe particles within the vapour-deposited rims of the olivine grains (Fig. 2.2b) similar to those observed in the lunar regolith by Keller and McKay (1993). The work of Sasaki et al. (2001) confirmed Hapke's vapour deposition model and it finally became the generally accepted model for lunar space weathering. The processes and products of weathering are summarized in Fig. 2.3.

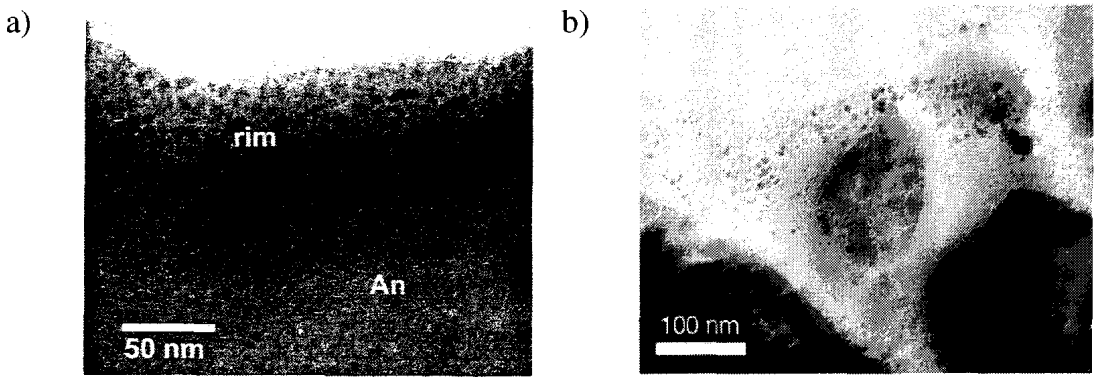

Figure 2.2: SMFe observed in vapour deposited grain coatings, confirming the vapour deposition model of lunar space weathering. a) Lunar soil sample (Hapke 2001). b) Laser irradiated olivine sample (Sasaki et al. 2001).

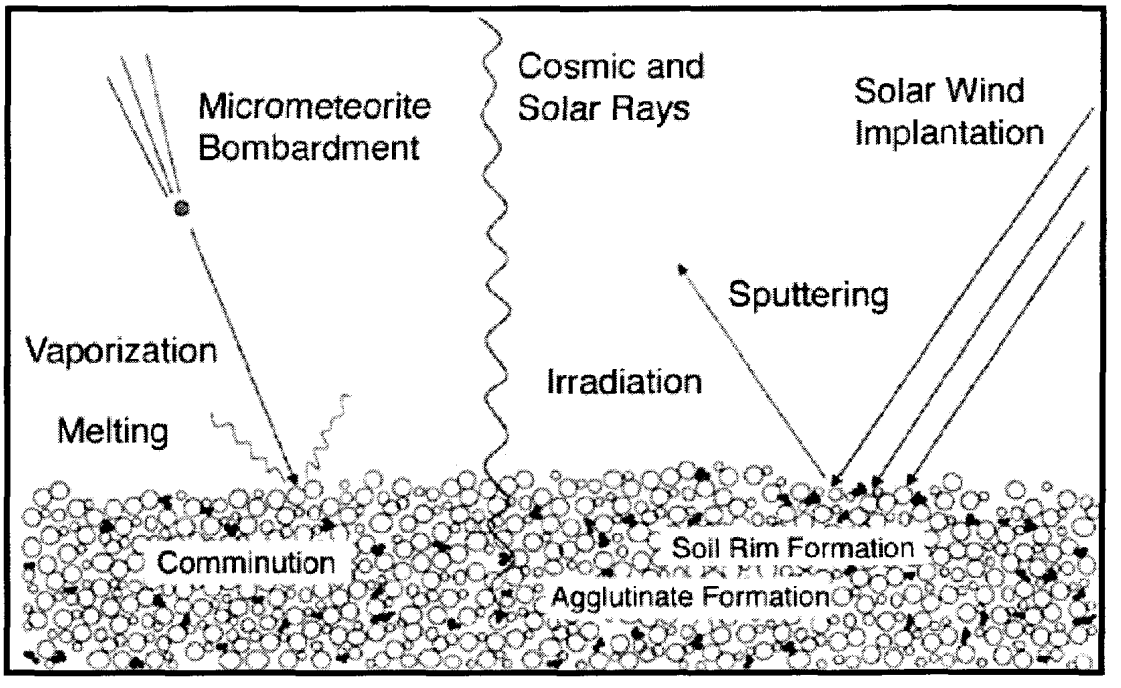

Figure 2.3: The processes and products of space weathering (Noble 2005).

The dominant processes which generate the vapour condensates are solar wind sputtering and micrometeorite impacts, both of which operate in the Main Belt. Micrometeorite bombardment is likely less effective compared to lunar weathering due to the lower impact velocities, so little melting or vapourization would occur. In addition, though impact velocities in the asteroid belt are lower, the rate of impact is higher, resulting in more comminution/pulverization and therefore fewer products of weathering (Noble et al. 2004). Solar wind sputtering would still play a role, though at a reduced rate due to the increased distance from the sun.

It has been more difficult to characterize the processes and products of asteroid weathering because we do not have asteroid regolith samples to study directly. Remotely obtained spectral data has shown evidence for weathering effects on asteroids but trends differ from lunar-like weathering and are challenging to interpret (Clark et al. 2002).

2.2 Laboratory Simulations

The initial motivation for asteroid weathering experiments was to resolve the S-type conundrum (see section 1.1.4). Those experiments, summarized in the following sections, revealed that weathering in the asteroid belt is far more complex than lunar-like weathering and that much more work needed to be done to characterize it.

2.2.1 Laser Shots

The first true simulation of weathering on OC meteorites was carried out by Moroz et al. (1996), who used pulsed laser shots to simulate impact melting and repeated crystallization of asteroid surfaces. Powdered ordinary chondrite samples were irradiated in vacuum by a pulsed laser. Moroz et al. (1996) found that the overall reflectance and spectral contrast were reduced, the slope was noticeably increased, and band area ratios decreased – all changes that would be characteristic of space weathering effects. Comparison of the modified meteorite spectra to those of S-type asteroids revealed that OC spectra could be modified to resemble the spectra of S-types, though a perfect match could not be obtained.

A particularly interesting result of this study was that, in addition to the other spectral changes observed, Moroz et al. (1996) observed a shift in the short wavelength Fe^{2+} absorption band to longer wavelengths, suggesting that olivine enrichment occurred in the samples during irradiation. Prior to this work, it had always been thought that band centre wavelengths, used to infer surface mineralogy, could not be affected by weathering processes. Thus Moroz et al. (1996) showed that space weathering was more significant to our interpretation of remote spectra than was previously believed, though their experiment was later criticized by Yamada et al. (1999) for not being a realistic simulation of micrometeorite impact.

In their experiment, Moroz et al. (1996) used a laser pulse duration of 0.5 – 1.0 μs, 1000 times the actual timescale of 1 – 10 μm micrometeorite impacts, according to Yamada et al. (1999). In a separate experiment, Yamada et al. (1999) irradiated powdered meteorite samples of various mineral compositions using a

more realistic pulse duration of 6 – 8 ns. They found that the reflectance of olivine-rich samples changed more dramatically than those of the pyroxene-rich samples for the same amount of irradiation. Hiroi and Sasaki (1999) performed a similar experiment and found that the degree of weathering modification was dependent on the olivine/pyroxene ratio of the sample, and that a higher olivine abundance leads to stronger degrees of weathering. Yamada et al. (1999) also used their experiment to estimate a timescale for weathering: assuming that the pulse frequency of the laser is comparable to the relative weathering timescale, pulse durations on the order of a nanosecond would correspond to timescales on the order of 10^9 years for weathering by micrometeorite impact.

The strong response of olivine to weathering effects was further explored by Hiroi and Sasaki (2001), who reproduced that finding in a pulsed laser experiment, then compared the results to spectra of several S, A, R, and V-type asteroids (which are all silicate-rich). Hiroi and Sasaki (2001) showed, for the first time, that the effect was present in asteroid spectra – the more olivine an asteroid's surface possessed, the redder the 1 μm band continuum appeared, indicating that olivine weathers more rapidly in space as well. In addition, Hiroi and Sasaki (2001) were the first to suggest, using spectral slope and band area ratios, that asteroids may be limited in the degree of weathering they can exhibit, i.e. at some point, they will reach saturation. They suggested that this could be due to the short life of surface regolith on asteroids, which is refreshed in numerous ways throughout a body's lifetime.

During these years, there was still much uncertainty about the actual processes causing the spectral modifications, despite Hapke's (2001) insistence on the vapour deposition model. In a pulsed laser experiment by Sasaki et al. (2001), Hapke's theory was finally validated when TEM analysis revealed the presence of SMFe on irradiated grains of olivine. Sasaki et al. (2001) considered this the missing link in the S-type conundrum. They also estimated a timescale for weathering caused by dust-impact heating of 10^8 years, consistent with the earlier Yamada et al. (1999) value of 10^9 years.

Earlier, Moroz et al. (1996) demonstrated that OC spectra could be modified in the direction of S-type asteroids. Sasaki et al. (2004) attempted to show the same effect using a shorter, more realistic pulse frequency. They were successful in darkening and reddening the spectra of their OC meteorite samples. They were also able to change the spectrum of a sample of the Allende meteorite, a carbonaceous chondrite, though not as dramatically.

In another pulsed laser experiment involving olivine samples enriched with metallic iron powder, Ueda et al. (2005) found that changes in the reflectance spectra were enhanced when metallic iron was present in the regolith. They suggested that the rate of weathering may be higher than previously estimated, especially on asteroids that contain metallic iron as a major mineral. This was a particularly significant result in terms of the S-type conundrum since metallic iron is common in OC meteorites.

Thus far, no one had yet taken into account thermal processes in their simulations. Brunetto et al. (2006) pointed out that at high laser light intensities in

pulsed laser simulations, the laser becomes a heat source for the material being observed. The change in temperature of the material can change its optical properties and can result in thermal material ablation, which is the dissipation of heat by melting (the streak of light seen when a meteor passes through the atmosphere is an example of this). Such an effect had not yet been considered, so Brunetto et al. (2006) investigated the potential significance of a thermal process in space weathering effects. To do this, they used pulsed laser irradiation to simulate micrometeorite bombardment on powdered silicates at energies above and below the ablation threshold. Brunetto et al. (2006) found that space weathering primarily affected the spectral slope and was stronger and more efficient above the ablation threshold, indicating that a thermal process was somehow involved in weathering. Based on their results, Brunetto et al. (2006) estimated a weathering timescale of 10^8 years with ablation, consistent with previous work, and determined that while irradiation below the ablation threshold can produce spectral modifications, the timescale required to do so would exceed the age of the solar system. They concluded that micrometeorite bombardment can only be properly simulated by laser irradiation if congruent laser ablation is considered.

Space weathering has long been known to be a surface process, affecting the smallest particles of regolith (Pieters et al. 1993). When there are particulate materials on the surface, evaporated material can condense on the surfaces of those particles to form amorphous rims containing SMFe. An experiment using a pulsed laser to irradiate flat mineral surfaces found no spectral change, implying that a surface regolith is actually necessary for modification by space weathering (Saski et

al. 2006). Prompted by Hyabusa measurements of Itokawa which appeared to contradict this finding (see section 2.3), Sasaki et al. (2006) carried out new experiments to further explore the idea. They irradiated both meteorite pellet samples and flat cut surfaces to compare the effects of weathering by micrometeorite impact. They observed significant spectral changes for each sample. Sasaki et al. (2006) also performed pulse laser irradiation on fresh meteorite samples left in their original, rocky form. They found that the rocky meteorite surfaces were also darkened and reddened by the simulation, though the effects were weaker than the modifications seen in the powdered samples. They concluded that while surface regolith significantly enhances the degree of weathering observed on a body, the microporosity of rocky surfaces may also allow weathered coatings to form without regolith.

2.2.2 Ion Irradiation

Ion irradiation experiments are used to simulate the effects of weathering by solar wind ion bombardment. Typically, H^+ and He^+ ions are used at keV energies. Such experiments have been conducted on freshly pulverized lunar rock samples to show how their spectra can be modified by weathering to resemble that of lunar soils (Hapke 2000, 2001). Based on such experiments, Hapke (2001) determined that it would require 10^5 years to darken lunar rocks by solar wind sputtering. He then reasoned that, because the ion flux is a factor of 10 less in the asteroid belt but only 1/20 as much SMFe is required to match the spectra of OC meteorites and S-type asteroids (0.025% as opposed to 0.5%, determined by applying a mathematical

model to an OC spectrum. See Hapke 2001 for a detailed derivation of his model), the required exposure time for asteroids in the Main Belt should be 50, 000 years. This is several orders of magnitude less than estimates derived from pulsed laser simulations, suggesting that the solar wind is more efficient at weathering surface regolith. Hapke (2001) does note, however, that the actual time is likely much longer because impacts continuously bury exposed regolith and bring fresh material to the surface.

While irradiation with H^+ and He^+ was seen to modify spectra, the changes were typically small. To simulate the effects of heavy particle irradiation, Strazzulla et al. (2005) irradiated an OC meteorite sample with 60 keV Ar^{2+} ions. The meteorite spectrum was progressively reddened in the direction of S-type asteroids. Strazzulla et al. (2005) estimated weathering timescales of $10^4 - 10^6$ yr at 1 AU and suggest that this is a more efficient mechanism for weathering in the near Earth environment than irradiation by lighter ions or micrometeorite bombardment.

To further investigate the physical mechanism behind Strazzulla et al.'s (2005) findings, Brunetto and Strazzulla (2005) carried out ion irradiation experiments on silicate meteorite samples using a range of light to heavy ions. They discovered that the heavy ions caused displacement of atoms in the uppermost layer microcrystals of the regolith and that this was more efficient at modifying the spectral slope of their samples across the 1 μm band than vapour coating by micrometeorite impact at 1 AU. Brunetto and Strazzulla (2005) also estimated a weathering timescale $< 10^6$ yr but noted that the time would vary depending on location in the solar system.

2.3 Direct Observation

The strongest evidence that space weathering operates in the Main Belt came from Galileo images of asteroids (951) Gaspra and (243) Ida, both S-type asteroids. The Galileo spacecraft encountered Gaspra on October 29, 1991 and took several images that were used to study colour variation across its surface. Colour differences across the entire asteroid were only 5% but local differences approached 30% (Chapman 1996; Fig. 2.4). There was an obvious correlation between colour and elevation: the bluer, "fresher" units were typically seen on ridges and small, fresh craters while redder units were located on lower, flatter areas of the surface (Chapman 1996). The imaging team concluded that there exists a process which changes Gaspra's colour over time, converting blue units to red and that older material will tend to migrate downhill (Chapman 1996).

On August 23, 1993, Galileo had an encounter with (243) Ida, where the colour variations were found to be even more prominent than on Gaspra (Chapman 1996). Chapman (1996) compared the spectra of three different terrains on Ida: blue, red, and neutral coloured (Fig. 2.5). He found that the spectra show the expected weathering continuum – a progression towards redder, darker spectra. Several lab experiments have attempted to convert OC meteorites into S-types and Chapman (1996) observed that the spectra of the various regions on Ida spanned a large fraction of the range required to make that conversion. As a result, Chapman (1996) concluded that S-type asteroids could be OC parent bodies and because Ida is a member of the Koronis family, perhaps the Koronis family is made up of OC-like asteroids.

Another spacecraft, NEAR Shoemaker, spent a year in orbit around (433) Eros, another S-type asteroid. While Eros did show evidence of weathering processes on its surface, the modifications observed were not what would be expected for lunar-like weathering (Clark et al. 2001). The spectral variations were very low, 4 - 8 %, while albedo contrasts of up to 40% were observed on Pysche crater (Clark et al. 2002). The lack of strong reddening of the spectrum is attributed to the enhanced presence of troilite (FeS), a dark, spectrally neutral component (Clark et al. 2002).

Most recently, the Hyabusa spacecraft has been used to characterize weathering on Near Earth asteroid (25143) Itokawa and has changed our understanding of weathering. Earlier work had suggested that surface regolith was necessary for modification by weathering (Sasaki et al. 2006). Itokawa's surface is characterized by dark boulders without fine regolith (Sasaki and Hiroi 2008), yet colour and albedo analyses of images taken by Hyabusa show significant variations that mimic weathering of ordinary chondrites (Abe et al. 2006), suggesting that the rocks on Itokawa have a thin, weathered layer. The Itokawa observations prompted Sasaki et al.'s (2006) work showing that the microporosity of rocks may allow rocky surfaces to exhibit weathering effects as well. Saito et al. (2006) estimate that weathering on Itokawa should have proceeded with a timescale of 10^7 years.

Figure 2.4: High-resolution image of (951) Gaspra, showing the subtle colour variations present on its surface (NASA/JPL). Bluish areas are typically correlated with fresh craters and ridges.

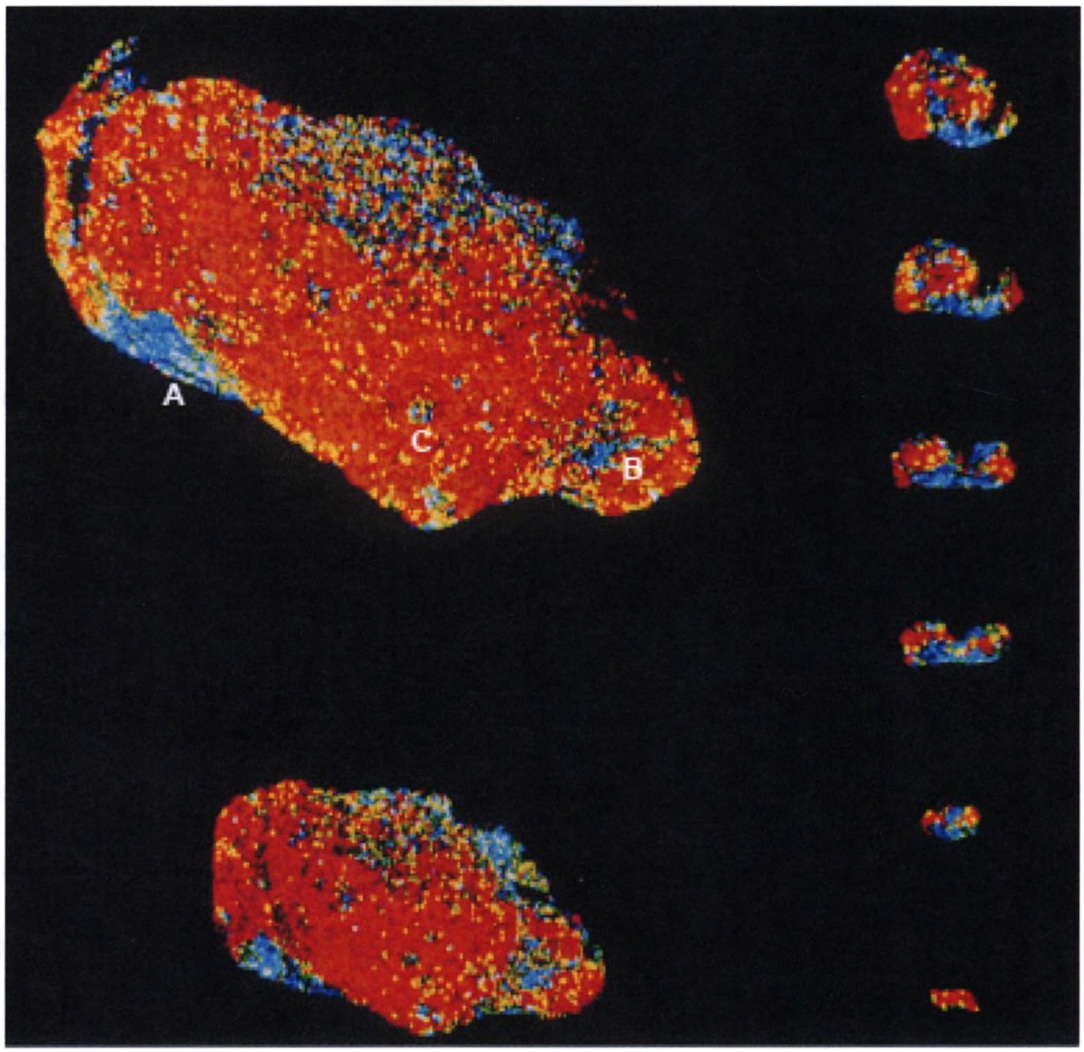

Figure 2.5: False colour images of (243) Ida showing pronounced colour variations on the surface. Terrains A, B, and C are indicated in the top left image (Veverka et al. 1996).

2.4 Remote Observations and Models

2.4.1 Trying to Resolve the S-type Conundrum

While some researchers were attempting to resolve the S-type conundrum through lab simulations, many more tried to find the OC parent bodies through ground-based observations of asteroids and worked to characterize weathering effects through asteroid spectra.

First to establish the presence of OC material in the Main Belt were Binzel et al. (1993b) who discovered, during the first phase of SMASS, that asteroid (3628) 1979 WD has a reflectance spectrum that is nearly identical to that of an LL6 ordinary chondrite. This finding did not put the issue to rest, however, because OC material in the Main Belt was still very rare and (3628) 1979 WD was estimated to be only ~7 km in diameter – small enough that it may be a "fresh" fragment that has not been exposed to the space environment very long. The possibility that its spectrum would eventually be modified to resemble that of an S-type asteroid remained open.

To get a clearer handle on the spectral mismatch, Fanale and Clark (1993) identified three numerical values pertaining to the spectral characteristics of S-type asteroids and OC meteorites, all of which would have to match in order to be able to conclude that OCs are derived from S-type asteroidal parent bodies. Those values are the 1 μm absorption band, the reflectance at 0.56 μm, and the slope of the continuum. Fanale and Clark (1993) evaluated the commonality of 23 OC meteorites and 39 S-asteroids by looking for overlap in their albedo vs. band depth, band depth vs. slope, and slope vs. albedo. They found no overlap between the two populations

and discussed the possibility that OCs, while mineralogically similar to S asteroids, are actually derived from a population of bodies that are too small to be observed and therefore are not included in our library of asteroid spectra. They did not consider weathering processes and did not attempt to modify the OC samples.

At the same time, Gaffey et al. (1993) were looking for evidence in S-type asteroid spectra that weathering processes were taking place on their surfaces and how they may work. They analysed reflectance spectra of 39 S asteroids and found evidence of size-dependent weathering processes. For asteroids with diameter < 100 km, Gaffey et al. (1993) observed that the absorption band is a strong function of diameter, with the two being anticorrelated (i.e. the absorption band increases steeply as the diameter decreases). They also observed a weak negative correlation of spectral slope with asteroid diameter, with the exception of the S(IV) sub-type (thought to most closely resemble OC spectra), for which they observed a strong negative trend. No correlation was found between diameter and albedo. Despite the compositional diversity among S-type asteroids, Gaffey et al. (1993) found that all subtypes in their dataset conformed to the observed trends. The results of this work were significant because once it was established that regolith maturity was correlated with body size, it became possible to test several weathering and regolith processes.

In an extension of Gaffey et al.'s (1993) results for Main Belt asteroids, Rabinowitz (1998) analysed data from an ongoing spectrophotometric survey of NEAs and observed a dependence on both size and orbit for asteroid colours. Rabinowitz (1998) found that most bodies > 2 km have reddish colours that are

similar to S-type asteroids while the smaller bodies have more neutral colours. In addition, the fraction of observed NEAs with S-type colours decreases for semimajor axis > 2.3 AU and the spectra begin to resemble those of C-type asteroids or OC meteorites. Essentially, there is a continuum present that Rabinowitz (1998) concluded could be explained by space weathering and may show that OC spectra are being modified to look like S-type asteroid spectra. Earlier work by Binzel et al. (1996) showed a similar continuum, with a transition from the fresh OC-like spectra of Q-type asteroids towards the redder spectra of S-types within the NEA population. Q-type asteroids are small, fast rotators and therefore have posed a challenge to observers trying gauge whether or not they may be the true OC parent bodies.

In a more in-depth analysis, Binzel et al. (2004) found that S- and Q-type asteroids have identical Main Belt source region profiles, implying related origins. In addition, they found that the transition from Q-type to S-type spectra is size dependent over a range of 0.1 to 5 km. On a plot of spectral slope vs. diameter, the slope asymptotically approaches 0.44 μm^{-1} for bodies > 5 km (Binzel et al. 2004). That value corresponds to the mean spectral slope of all Main Belt asteroids within SMASSII, prompting Binzel et al. (2004) to suggest that perhaps it represents a critical limit for weathering. If so, this would confirm Hiroi and Sasaki's (2001) prediction that a body is limited in the degree of weathering it can exhibit. Together, the work of Rabinowitz (1998) and Binzel et al. (1996, 2004) gave more weight to the idea that S-types may be the weathered parent bodies of OC meteorites, though issues still remained.

To resolve some of the lingering doubts, Pieters et al. (2000) extended Hapke's vapour deposition model from the lunar surface to S-type asteroids and demonstrated that the observed spectra of S-types are actually a natural consequence of the space weathering of semi-transparent minerals. Through lab experiments, Pieters et al. (2000) demonstrated that SMFe is produced on surface grains of lunar soils by vapour deposition and irradiation. They noted that optical properties of the soils were highly dependent on the cumulative amount of SMFe present in the soil, which can vary with initial composition and location in the Solar System (see Noble et al. 2004 and 2007 for detailed analyses of the optical effects of SMFe). Pieters et al. (2000) then modeled the effects of small amounts of SMFe on grains of OC regolith, effectively weathering the OC samples, and compared the resulting spectral properties to those of S-type asteroids. They demonstrated that S-type spectra directly mimicked the effects of their weathered OC regolith, concluding that the inferred S-type mineralogy is compatible with theoretical OC parent bodies. Like Sasaki et al. (2001), Pieters et al. (2000) argued that this was the missing link to resolving the S-type conundrum. The remaining issue now, according to Pieters et al. (2000), was determining a weathering rate.

2.4.2 Toward a General Model

Earlier lab simulations were able to estimate weathering timescales but the first estimate of a space weathering rate came from Jedicke et al. (2004). As both Jedicke et al. (2004) and Chapman (2004) point out, it is challenging to arrive at such a rate with any certainty; in a lab, it is difficult to ensure that the techniques

used in simulating the weathering process are appropriately calibrated with the actual presumed mechanism (the unrealistic pulsed laser frequency of Moroz et al. 1996 in the first simulation attempted is an example of this issue). In addition, spacecraft instruments can distinguish the relative ages of terrains but it is difficult to obtain an absolute surface age. Jedicke et al. (2004) developed a method for measuring the rate of space weathering on Main Belt S complex asteroids using the relationship between asteroid colours and their dynamical ages.

As discussed in Chapter 1, asteroid families are the result of a catastrophic disruption. In theory, the surfaces of asteroids in a family should all have the same age since it was "reset" at the time of disruption. This is the dynamical age, but it is only a limiting value since, throughout the lifetimes of family members, other events may have modified their surfaces (Jedicke et al. 2004; Binzel et al. 2004; Bottke et al. 2005).

For their study, Jedicke et al. (2004) used asteroid colours from the Sloan Digital Sky Survey Moving Object Catalog (SDSS MOC) and assumed that the dynamical ages of the families represented the surface ages of their member asteroids. They demonstrated that there is a size dependent component to asteroid colours, which also varied with mineralogical differences. Jedicke et al. (2004) developed a formula for change in colour as a function of time using Principle Component Analysis and also derived a characteristic weathering timescale of $10^{10.4 \pm 0.2}$ yr. They noted that this was two orders of magnitude larger than lab estimates, attributing the difference to the lack of sensitivity of their method to components of the weathering process that may occur on timescales of $< 10^6$ yr as

there was no data for very young families with well measured ages. Jedicke et al. (2004) extrapolated their age-colour relationship to very young ages and found a good match to the colour of freshly cut OC meteorite samples, providing more evidence in favour of an association between them and S-type asteroids. Recently, Willman et al. (2008) corrected the weathering rate determined by Jedicke et al. (2004) using new observations of young Iannini and Karin family members. The revised timescale, 570 ± 220 My (~10^8 yr), is in better agreement with lab measurements.

Building on the work done by Jedicke et al. (2004), Nesvorný et al. (2005b) carried out a much more comprehensive study using data from SDSS and included younger families. Using Principal Component Analysis, they showed that PC1 (the first principal component) was effectively a measure of the spectral slope between 0.35 and 0.9 μm, then looked for correlations between PC1 and various parameters including asteroid size, distance from the sun, and dynamical age. Nesvorný et al. (2005b) found that the only statistically significant correlation was with family age. They determined that for $2.5 \leq t \leq 3000$ My, where t is the age in My, the spectral slope changes due to space weathering at a rate of 0.1 μm^{-1} x $\log_{10} t$. Nesvorný et al.'s (2005b) relation suggests that the rate of weathering is greatest for freshly exposed surfaces and as an object ages, it has less opportunity for more weathering on its already weathered surface. This is in agreement with the findings of Hiroi and Sasaki (2001) and Binzel et al. (2004).

The most convincing evidence for weathering to date (per Chapman 2004) is the large colour difference that Nesvorný et al. (2005b) observed between Koronis

family members and Karin members, with Koronis asteroids being significantly redder. Both families are believed to be from the same progenitor (in the sense that the Karin cluster was formed through the catastrophic disruption of a Koronis member), but the difference could not be explained with an assumed size dependence so Nesvorný et al. (2005b) attributed it to the difference in age and degree of weathering between the families. The difference between Karin and Koronis members resembles the Q-type to S-type spectral continuum observed by Binzel et al. (1996, 2004).

Despite a lack of significant correlation with distance from the sun in Nesvorný et al.'s (2005b) work, Marchi et al. (2006) argued that because some of the physical processes of weathering are related to distance from the sun, the properties of weathering must also depend in some way on that distance. In their analysis of S-type asteroids, Marchi et al. (2006) found that mean asteroid slope increased with age, and that the correlation held for NEAs and Main Belt asteroids < 2.7 Gy old. Over 2.7 Gy, the slope was almost constant, which may be evidence of saturation. The slope-age relation was consistent with Binzel et al.'s (2004) findings for NEAs. Looking at spectral slope vs. distance from the sun, NEAs showed a positive correlation, while Main Belt asteroids showed an anticorrelation. Because they were able to find a unique and general slope-exposure relation valid for the entire S complex, Marchi et al. (2006) suggested that Sun-related effects must dominate space weathering processes.

Most recently, Mothé-Diniz and Nesvorný (2008) shifted their focus to extremely young asteroid families and found that asteroids < 1 My are only partially

weathered. Q-type asteroids have already been shown to be the best proxy for OC material and while Binzel et al. (1993b) found evidence for OC material in the Main Belt, Mothé-Diniz and Nesvorný (2008) found Q-type asteroids in the Main Belt for the first time. This may represent a new stepping stone on the path to finally resolving the S-type conundrum.

Chapter 3

Data Collection

3.1 Target Selection

As has been described in the previous chapters, asteroid families are useful in studies of physical processes and asteroid evolution because of their common origin. The Koronis family is particularly advantageous from a space weathering perspective; surface ages of asteroids are impossible to determine without *in situ* measurements but the dynamical age of this family is known, giving an upper limit to the surface exposure age of its members. In addition, their common origin implies that they are compositionally similar. The presence of the much younger Karin cluster is useful as it provides a broad range in surface age for potential targets and thus observations of Koronis members along with Karin members can be used to constrain weathering timescales. In addition, this family has been studied in the context of space weathering by other groups using different techniques (e.g. Binzel et al. 1993; Nesvorný et al. 2005b) and those studies can provide a basis for comparison with the ECAS results.

In May and September 2007, Koronis family asteroids were observed using the 1.8 m Plaskett Telescope with an EEV-1 CCD detector at the Dominion Astrophysical Observatory (DAO) in Victoria, British Columbia (see Table 3.1 for filter characteristics). Six nights of data were taken at DAO in May, of which only the final night was used in this study due to problems with the b and w filters on

preceding nights. Nine nights of data were obtained in September, of which seven were used (the other two were not suitable for all-sky calibrations). The observations are summarized in Table 3.2.

From June through August 2007, images were taken at the Elginfield Observatory (UWO) with the 1.2 m telescope in Cassegrain mode and using a Finger Lakes CCD detector. Due to various technical problems during the Elginfield observing campaigns and poor sky conditions throughout the summer, all-sky photometric calibrations could not be obtained for the Elginfield data. Consequently, no targets from that period have been included in this study.

The Koronis family is clustered near the outer middle of the Main Belt, with $a_p = 2.83 - 2.95$ AU, $e_p = 0.03 - 0.1$, and $\sin i_p = 0.035 - 0.045$ (Mothé-Diniz et al. 2005). Since a comprehensive list of all Koronis and Karin members does not currently exist, a script was written in MATLAB to search the AstDys database[4] for all numbered asteroids located within the Koronis family's proper orbital element space and use the results to generate a list of potential targets. The list generated in MATLAB was then compared against the JPL "Small Body What's Observable" database[5] before each observing run to determine which of the possible targets would be observable during the scheduled telescope time. For the purposes of this study, a target was considered "observable" if it was above 30° elevation for 30 minutes or longer, its apparent visual magnitude was brighter than +16 (Elginfield) or +19 (DAO), and it was at/close to opposition (when asteroids are typically brightest). When limiting magnitudes were taken into account, Karin cluster

[4] The Asteroids Dynamic Site: http://hamilton.dm.unipi.it/astdys/
[5] http://ssd.jpl.nasa.gov/sbwobs.cgi

members had to be excluded each month as all potential targets were too faint to be observed at Elginfield and sky conditions did not allow sufficient signal-to-noise for such faint targets at DAO.

3.2 Observing with ECAS Filters

The most commonly used filter system in astronomy is the Johnson-Cousins UBVRI, which has become the standard system in which photometric colours are reported (Warner 2006). There is likely to be at least one star in any given field of view that has a catalogued UBVRI colour. The ECAS filter system, on the other hand, is not a "standard" photometric system; though the filters were specially developed with band passes that target major features in asteroid spectra, the system is not widely used. As a result, calibration of the DAO data was dependent on observations of the ECAS standard stars defined and catalogued by Tedesco et al. (1982). In addition to the target asteroids, it was necessary to observe several ECAS standards each night in order to determine the appropriate equations that would transform the DAO instrument measurements to the established ECAS standard values. Since the asteroids observed were not in the same field or at the same airmass (see section 4.1.1) as the standard stars, all-sky photometric solutions were required (as opposed to differential, where only the difference in magnitude between targets in the same field is considered). The process of obtaining the all-sky solutions is described in Chapter 4.

Several challenges were encountered during the observing campaigns. First, high precision photometry is always difficult, particularly all-sky photometry as it is

highly sensitive to atmospheric conditions. Any presence of haze or high cirrus clouds in the field of view can translate into large errors in the photometric corrections and the colour terms obtained for each asteroid. While Victoria, B.C. was a more desirable location than Southwestern Ontario, it was still not an ideal site for such measurements. In addition, the filters themselves posed a challenge as the u and the w bands were near the sensitivity limits for the DAO detector. The u filter was especially sensitive to atmospheric variations and there was significant noise in that wavelength region, due to the detector. At the Elginfield Observatory, the u filter clouded over midway through the campaign and became unusable.

Filter	**DAO (μm)**	**Elginfield (μm)**	**Zellner et al. (1985b) (μm)**
u	0.370	unknown	0.359
b	0.450	0.4454	0.437
v	0.550	0.5488	0.550
w	0.700	0.7051	0.701

Table 3.1: Central wavelengths of ECAS filters used at DAO, Elginfield, and in the Zellner et al. (1985) ECAS dataset.

UT Date	No. Std. Fields	No. Asteroids	Filter	Remarks
20070522	6 (2)	7	u,b,v,w*	Only 1 asteroid useable
20070907	3 (n/a)	2	u,b,v,w	Not reduced; CCD not fully cooled and v. poor seeing, hazy
20070908	3 (1)	2	u,b,v,w	
20070909	3 (2)	2	u,b,v,w	
20070910	8 (3)	2	u,b,v,w	
20070911	8 (7)	2	u,b,v,w	Near photometric night
20070912	9 (7)	0	u	Near photometric night; took additional u exposures for targets from previous nights
20070913	9 (7)	2	u,b,v,w	
20070914	9 (n/a)	0	u	Not reduced; took additional u exposures for targets from previous nights but too hazy to see targets
20070915	3 (2)	3	u,b,v,w	1/3 targets could not be identified during data reduction

*During the May campaign, it was discovered after the run was complete that the w filter had been mistakenly switched with the p.

Table 3.2: Summary of observations. The second column gives number of unique standard fields observed each night and in brackets, the number of those fields used to determine the extinction coefficient.

3.3 Data Summary

3.3.1 DAO Dataset

During the DAO observing campaigns, a total of 21 Koronis family asteroids were observed, of which 12 were used for this study. The targets were selected so that there would be a spread in absolute magnitude, H, because H is a function of diameter and would correspond to a range in target size. In addition, smaller bodies are statistically younger so this would allow for a potential range in the surface ages of the targets. The absolute magnitudes of the Koronis members observed are H = 9.23 – 13.4, however it should be noted that there is a paucity of targets with H = 10.5 – 12.5. The majority of targets in that range were observed at Elginfield and during the May DAO campaign; they were ultimately rejected due to the various technical issues described in the previous section. The targets used are a fair sample

of the Koronis region of the Main Belt (Fig. 3.1), though the range in their orbital elements is likely too narrow to allow any definitive conclusions to be drawn regarding the relationship between a_p, e_p, i_p and space weathering.

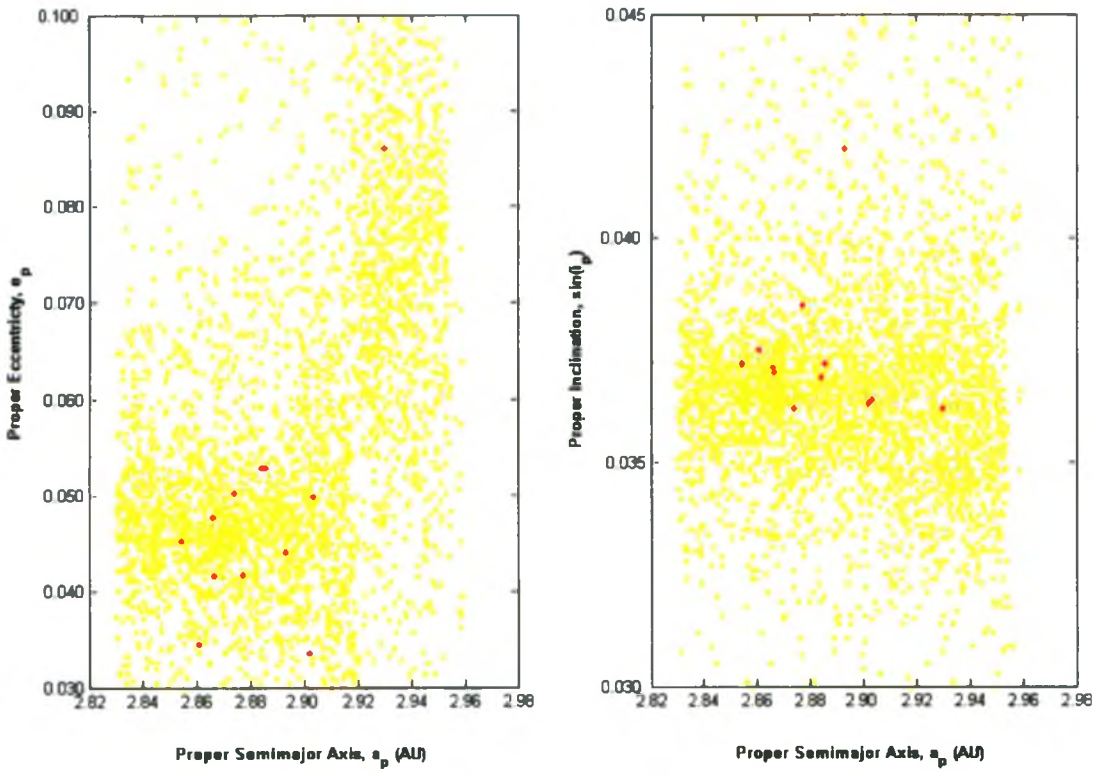

Figure 3.1: Distribution of observed Koronis members (red dots) in a_p, e_p, i_p space against background family members (yellow dots).

3.3.2 1985 ECAS Results

In addition to the new observations, this study also made use of the results of the 1985 Eight Colour Asteroid Survey (Zellner et al. 1985b), which were obtained from the NASA Planetary Data System[6]. The 1985 data were used to validate the results from the DAO observations as well as to allow for generalization of those results to a broader population. Zellner et al. (1985b) present results for 589 minor

[6] http://pds.jpl.nasa.gov/

planets distributed throughout the solar system, from NEAs to the Jupiter Trojans. The survey divided the asteroids into 18 orbital element zones (as defined in Zellner et al. 1985) and analysed the reflectance spectrum of each asteroid to determine the distribution of spectral types within the zones. For the purposes of this study, only the populations that were determined to be predominantly S-type were used (Table 3.3). Where targets were observed multiple times, the weighted means given in Zellner et al. (1985b) were used in calculations.

The Koronis zone, containing the Koronis family, is included in this dataset. Of the thirteen member asteroids observed by Zellner et al. (1985b), three overlap with the DAO dataset and were used for comparison. The agreement between DAO results and those of Zellner et al. (1985b) is discussed in the following chapter.

Zone	No. Asteroids	Abs. Mag. H	Mean Semimajor axis, a* (AU)
Apollo-Amor-Aten (NEOs)	9	9.45-18.97	1.831
Floras	35	7.00-12.75	2.230
Phocaeas	8	7.83-12.68	2.368
Main Belt I	32	6.50-11.85	2.391
Koronis	13	9.23-11.57	2.873
Eos	15	9.18-10.43	3.014

*Osculating semimajor axis.

Table 3.3: Summary of Zellner et al. (1985b) data, by orbital element zone.

Chapter 4

Data Reduction & Analysis

4.1 All-Sky Photometric Calibration

The data reduction process consisted of several steps: the application of photometric corrections, aperture photometry to measure the instrument magnitude of each target, determination of nightly extinction coefficients for each filter, derivation of nightly transform equations for each filter, and application of the transforms to obtain asteroid colour terms. Those colour terms were then converted into the spectral reflectance values necessary to calculate Hiroi et al.'s (2006) inflections.

Before any measurements were made with the images, the standard photometric corrections (removal of bad pixels, biases, flat fields) were applied. The majority of images were detrended by David Balam at the University of Victoria using an Image Reduction and Analysis Facility (IRAF) script, while the remainder was done at UWO using IRAF's ccdproc routine.

4.1.1 Extinction Correction

After all images were detrended, aperture photometry was done with IRAF's apphot routine to obtain instrument magnitudes for each standard star. Aperture photometry measures the light flux within an aperture of user-defined pixel size and converts it to an apparent visual magnitude, in the instrument system. The aperture

radii used were typically between 9 and 12 pixels, ~2 to 3 times the full width at half max. of the point spread function for the standard stars (dependent on nightly seeing).

Next, the instrument magnitudes were corrected for atmospheric extinction effects. All ground-based telescopes must look through Earth's atmosphere, which can absorb and scatter light from the target so that the flux received at the telescope is less than what would be measured outside of the atmosphere. This dimming effect is called extinction. The amount of atmosphere a telescope is looking through is measured in airmasses; if the telescope is pointed straight up, it is looking through one airmass (the minimum path length through the atmosphere) and airmass increases as the telescope is pointed at lower elevations (Romanishin 2006). The airmass of any target is given by:

$$X = \sec(\theta_Z) - \Delta X \tag{4.1}$$

where θ_Z is the zenith angle of the target and

$$\sec(\theta_Z) = \frac{1}{[\sin\lambda\sin\delta + \cos\lambda\cos\delta\cos h]} \tag{4.2}$$

which represents a plane-parallel approximation of the airmass (Romanishin 2006). In the above equation, λ is the latitude of the observatory, δ is the declination of the target, and h is the hour angle of the target at the time of the observation. The latitude used for the DAO was 48.52° N and all other parameters were read from the image headers. In equation (4.1), ΔX corrects for the curvature of the Earth and is given by

$$\Delta X = 0.00186[\sec(\theta_z) - 1] + 0.002875[\sec(\theta_z) - 1]^2 + 0.0008083[\sec(\theta_z) - 1]^3 \quad (4.3)$$

(Romanishin 2006). Airmasses were calculated using either an IRAF script (on images detrended by D. Balam) or a MATLAB script (on images detrended at UWO). Quantitatively, extinction is the change in magnitude per unit of airmass. It can be found graphically by taking the slope of a plot of instrument magnitude vs. airmass. This value is also called the extinction coefficient, K, and it allows us to determine the "true" brightness of a target above the Earth's atmosphere.

Extinction coefficients were determined each night for all four filters. A plot of instrument magnitude vs. airmass was generated for every standard field that was observed multiple times throughout the night and the median of all extinction values for each filter was used as the nightly extinction coefficient for that filter (Table 4.1). Some values were rejected during this portion of the analysis, assuming a Gaussian distribution and applying the Chauvenet criterion. Negative values were also rejected, as they are unphysical. The final values are comparable to those obtained by Tedesco et al. (1982), though somewhat higher, as would be expected given the difference in observing location and quality of sky conditions. The variation in extinction values from night to night and the variation in their errors reflect the changing sky conditions during the DAO campaign. Only two of the nights, September 10 and 11 (UT), were near to ideal. This sky variability was the largest source of error in this study, particularly for the u filter as that band is especially sensitive to changes in the atmosphere and it was at the lower limit of the EEV-1 detector's sensitivity.

UT Date	$K_u \pm \delta K_u$	$K_b \pm \delta K_b$	$K_v \pm \delta K_v$	$K_w \pm \delta K_w$	Remarks
20070522	1.012 ± 0.040	0.473 ± 0.045	0.201 ± 0.064	n/a	No w filter
20070908	0.797 ± 0.044	0.281 ± 0.063	0.95 ± 0.10	0.243 ± 0.464	Poor range in airmass
20070909	0.841 ± 0.145	0.300 ± 0.057	0.233 ± 0.066	0.080 ± 0.068	
20070910	0.811 ± 0.118	0.522 ± 0.080	0.21 ± 0.08	0.120 ± 0.044	
20070911	0.673 ± 0.049	0.325 ± 0.015	0.253 ± 0.018	0.128 ± 0.002	
20070912	0.622 ± 0.005	0.252 ± 0.009	0.154 ± 0.003	0.066 ± 0.004	
20070913	0.711 ± 0.057	0.297 ± 0.015	0.133 ± 0.033	0.038 ± 0.012	Poor range in airmass
20070915	0.692 ± 0.155	0.314 ± 0.014	0.259 ± 0.002	0.138 ± 0.121	Poor range in airmass

Table 4.1: Summary of nightly median extinction values.

4.1.2 Transform Equations

Extinction corrections were applied to the instrument magnitudes to obtain zero airmass (0 AM) instrument magnitudes, i.e. the instrument magnitude of the target if the telescope was looking outside of the atmosphere, via

$$m_I^{0AM} = m_I - XK \tag{4.4}$$

where m_I is the instrument magnitude, X is the airmass, and K is the extinction coefficient. Instrument colours at zero airmass were determined by taking the difference of the appropriate bands: $(u\text{-}v)_I^{0AM}$, $(b\text{-}v)_I^{0AM}$, and $(v\text{-}w)_I^{0AM}$. Positive colour terms indicate a "red" object.

The DAO instrument colours were related to the standard system colours of Tedesco et al. (1982) through a series of linear transform equations in each band:

$$\begin{aligned}(U-V)_E &= \alpha(u-v)_I^{0AM} + \beta \\ (B-V)_E &= \chi(b-v)_I^{0AM} + \varepsilon \\ (V-W)_E &= \gamma(v-w)_I^{0AM} + \eta\end{aligned} \tag{4.5}$$

where the left hand terms represent the standard ECAS colours (as defined by Tedesco et al. 1982), α, χ, and γ are the correlation terms and β, ε, and η are the zero

points for each band. If the instrument and the standard systems were identical, then $\alpha, \chi, \gamma = 1.00$ and $\beta, \varepsilon, \eta = 0.00$. The actual nightly values were found by plotting the Tedesco et al. (1982) catalogued colour term vs. the zero airmass colour term for each standard star, then using a least squares fit to find the slope and y-intercept. For the filter system used at DAO, $\alpha = 0.849$ to 1.082, $\beta = -4.365$ to -3.677, $\chi = 1.096$ to 1.907, $\varepsilon = -2.709$ to 0.117, $\gamma = 0.586$ to 0.946, and $\eta = 0.165$ to 0.703. While there was some variability in correlation terms from night to night, they were relatively consistent for each filter throughout the campaign; the largest variations were in the zero points. In general, the instrument colours transformed well to the standard system.

Unlike the colour terms described above, the apparent visual magnitudes reported by Tedesco et al. (1982) for the standard stars, as well as those reported for the minor planets in Zellner et al. (1985b) are in the UBVRI system (transformed using the catalogued values Landolt 1973 for stars in field SA 114 or Purgathofer 1969 for all others). The values reported in this paper follow the same convention. The V magnitude is given by

$$V = v_I^{0AM} + [V_{ZP}^0 + c(B-V)] \tag{4.6}$$

where v_I^{0AM} is the zero airmass instrument v magnitude, V_{ZP}^0 is the v-band zero point, c is the colour dependence on the (B-V) term and (B-V) is the catalogue value in either the Landolt or Purgathofer system. The values of c and V_{ZP}^0 were found by plotting $(V - v_I^{0AM})$ vs. (B-V) for each star and using a least squares fit. Unlike the c values reported by Tedesco et al. (1982), the dependence of the DAO filters on the

(B-V) term was not negligible; typical values of c were -0.30 to 0.11. The zero point, $V_{ZP}^{0} \approx 24.0$. In order to calculate the V magnitudes for the asteroids, for which Landolt and Purgathofer (B-V) terms were unknown, a nightly transform solution for $(b\text{-}v)_I^{0AM}$ to (B-V) was also found.

4.2 Asteroid Colours

Instrument colours were found for each asteroid following the method described in section 4.1.1. The nightly transform equations were then applied to obtain the standard ECAS colours (Table 4.2). The $(b\text{-}v)_I^{0AM}$ term was transformed to both the standard ECAS system, for comparison with the Zellner et al. (1985b) results, and the Landolt/Purgathofer system to allow a V magnitude to be calculated. Only $(B\text{-}V)_E$ is reported in Table 4.2. Multiple exposures were taken in each filter, so the values summarized here are averages. In cases where the SNR was not high enough to obtain a reliable instrument magnitude, images were stacked together and the resulting single measurement is reported in Table 4.2. No $(U\text{-}V)_E$ term is reported for (10240) 1998 VW34 and (14246) 2000 AN50 as there were no useable u filter images for those targets and no $(V\text{-}W)_E$ term is reported for (534) Nassovia as the w filter was not used during the May observing run.

The measured apparent visual magnitudes were in good agreement with the expected values given by the JPL Horizons ephemeris generator[7] for the times at which each asteroid was observed. The V magnitudes were also compared to those

[7] JPL Horizons: http://ssd.jpl.nasa.gov/horizons.cgi

reported by other observers for the same timeframe in the AstDys database and were found to agree.

Since the u, b, and v filters are comparable to the Johnson-Cousins UBV system, the (B-V) terms could be directly compared to those given in the JPL Small Body Database Browser for the first five asteroids in Table 4.2 (the JPL values are archived measurements by previous observers). No (B-V) terms were available for the other targets. The $(B-V)_E$ values in Table 4.2 are typically redder than the catalogue values but agree within the error bounds, with the exception of (658) Asteria. The $(B-V)_E$ term for this target is too high to be plausible and its associated error is also very high. Because the $(B-V)_E$ term was required to calculate both the C_b and C_v inflections, asteroid (658) Asteria was excluded from further analysis. Asteroids (3903) Kliment Ohridski and (14246) 2000 AN50 were also rejected on the basis of unrealistic $(B-V)_E$ values.

Several of the asteroids observed at DAO were also observed by Zellner et al. (1985b). They were (277) Elvira, (462) Eriphyla, and (1245) Calvinia. Comparing colour terms between the two datasets, values typically agreed within the error bounds. Differences are most likely due to the large variation in sky conditions between Victoria, B.C. and the University of Arizona, where the Zellner et al. (1985b) data was obtained.

Target	Obs. Date (UT)	H	$(U-V)_E$	$(B-V)_E$	V	$(V-W)_E$
277 Elvira	20070911	9.84	0.318 ± 0.250	0.175 ± 0.035	13.512 ± 0.073	0.112 ± 0.016
462 Eriphyla	20070910	9.23	0.383 ± 0.136	0.115 ± 0.017	13.283 ± 0.125	0.123 ± 0.008
534 Nassovia	20070522	9.77	0.271 ± 0.135	0.081 ± 0.014	14.149 ± 0.127	-
658 Asteria	20070908	10.54	0.371 ± 0.188	0.612 ± 0.330	13.963 ± 0.191	0.012 ± 0.064
1254 Calvinia	20070915	9.89	0.352 ± 0.105	0.217 ± 0.019	13.936 ± 0.019	0.104 ± 0.003
3903 Kliment Ohridski	20070908	12.00	0.328 ± 0.187	-0.099 ± 0.290	16.691 ± 0.141	0.167 ± 0.057
5428 1987 RA1	20070909	12.50	0.374 ± 0.067	0.059 ± 0.023	17.002 ± 0.105	0.159 ± 0.015
6299 Reizoutoyo	20070909	12.40	0.392 ± 0.142	0.105 ± 0.025	17.242 ± 0.099	0.158 ± 0.015
10240 1998 VW34	20070913	13.00	-	0.007 ± 0.012	18.062 ± 0.115	0.259 ± 0.007
14246 2000 AN50	20070910	13.00	-	-0.191 ± 0.038	17.288 ± 0.143	0.229 ± 0.007
14280 2000 CN72	20070911	13.20	0.409 ± 0.207	0.073 ± 0.031	17.701 ± 0.070	0.127 ± 0.016
14382 Woszczyk	20070913	13.40	0.271 ± 0.135	0.081 ± 0.014	17.221 ± 0.081	0.099 ± 0.007

Table 4.2: Summary of asteroid colour terms. All terms are in the ECAS system except for the V magnitudes, which are reported in the UBV system.

4.3 Spectral Reflectance

Photometric colours were converted to spectral reflectances using the equation

$$\log_{10} R_x = \pm 0.4 c_x \tag{4.7}$$

where R_x is the reflectance, normalized to R = 1 in the v band, and c_x is the colour term (Zellner et al. 1985b). The sign convention is negative for wavelengths shorter than the visual. Individual reflectance curves for each target (excluding those rejected in the previous section) are shown in Fig. 4.1, normalized to $R_v = 1.00$.

Where catalogued spectra were available for the same targets, either from the Zellner et al. (1985b) dataset or the SMASSII catalogue, they are included on the plots for comparison. The reflectance curves for Koronis members observed at DAO (Fig. 4.2) are comparable to those obtained by Mothé-Diniz et al. (2005) for wavelengths between 0.4 and 0.7 μm.

The DAO spectra are in good agreement with the Zellner et al. (1985b) and SMASSII spectra, though there is some deviation in the b wavelength region. Most curves have the expected shape for S-type asteroids, despite the fluctuations in the b band.

High errors in $(U\text{-}V)_E$ propagate into high R_u errors, making it a challenge to gauge how steep the slopes really are. The u band reflectance was unrealistically high for asteroid (14382) Woszcsyk and was rejected, so only the C_v inflection could be determined for this target.

The spectral reflectances were used to calculate the Hiroi et al. (2006) inflections for both the DAO targets and the Zellner et al. (1985b) asteroids, the final values needed to begin analysis of space weathering on these targets, using the equations

$$C_v = \frac{(1 - R_v / R_w)}{\lambda_w - \lambda_v} - \frac{(R_v / R_w - R_b / R_w)}{\lambda_v - \lambda_b}$$
$$C_b = \frac{(1 - R_b / R_v)}{\lambda_v - \lambda_b} - \frac{(R_b / R_v - R_u / R_v)}{\lambda_b - \lambda_u} \qquad (4.8\text{-}9)$$

where R_x and λ_x correspond to the reflectance and center wavelength (from Table 3.1), respectively, of filter band x (Hiroi et al. 2006).

a)

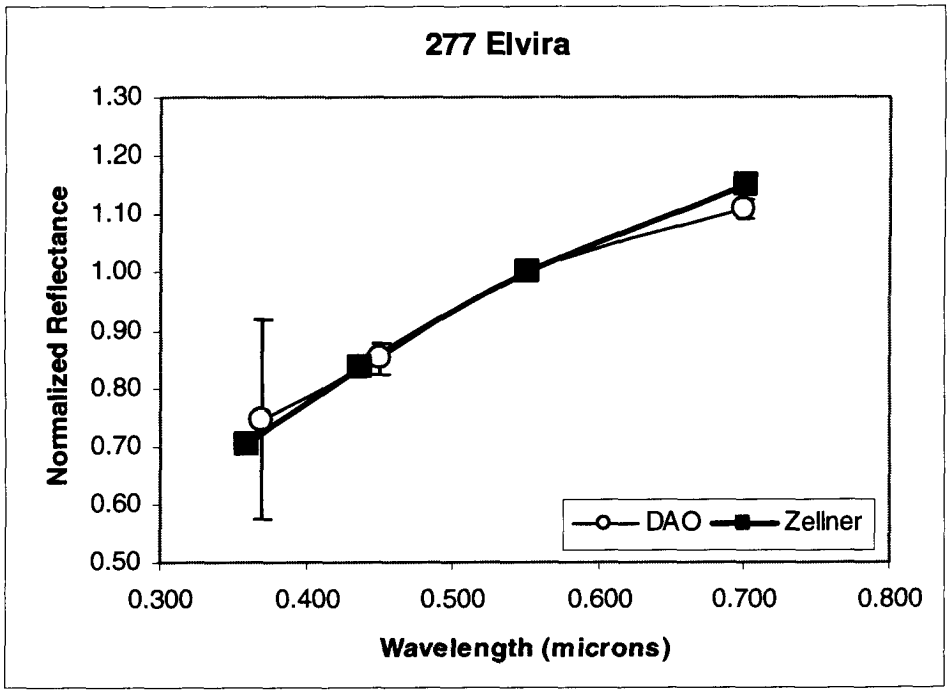

b)

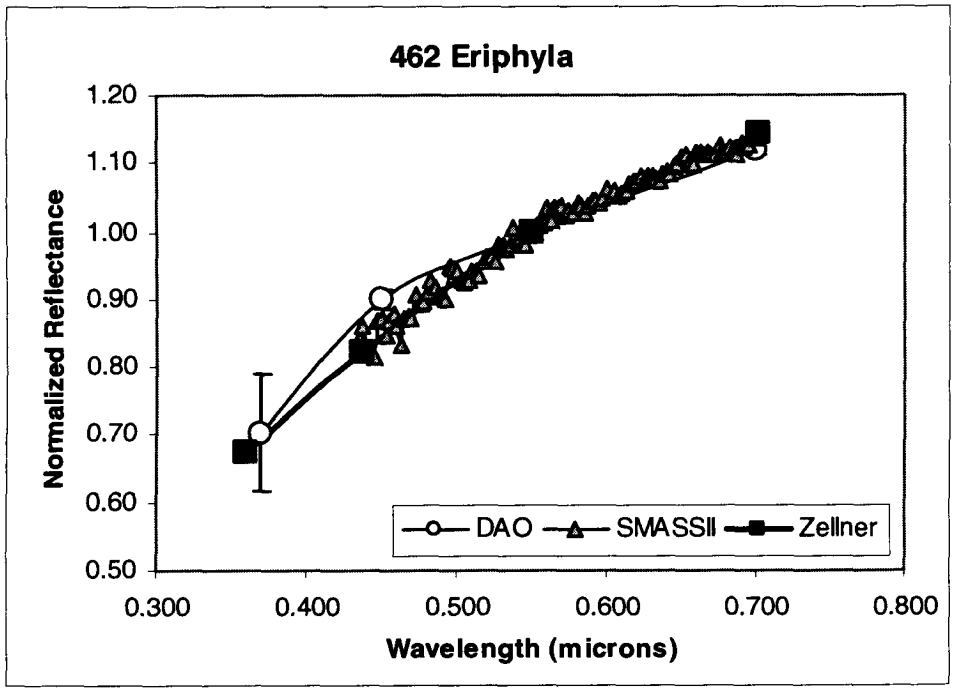

Figure 4.1: Reflectance curves for Koronis family asteroids observed at DAO.

c)

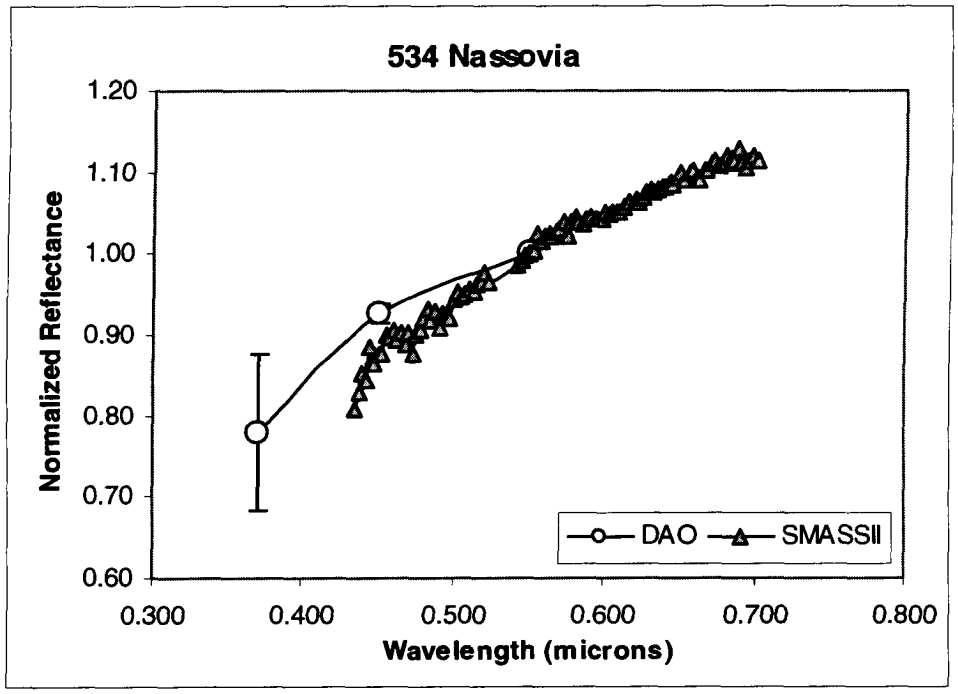

d)

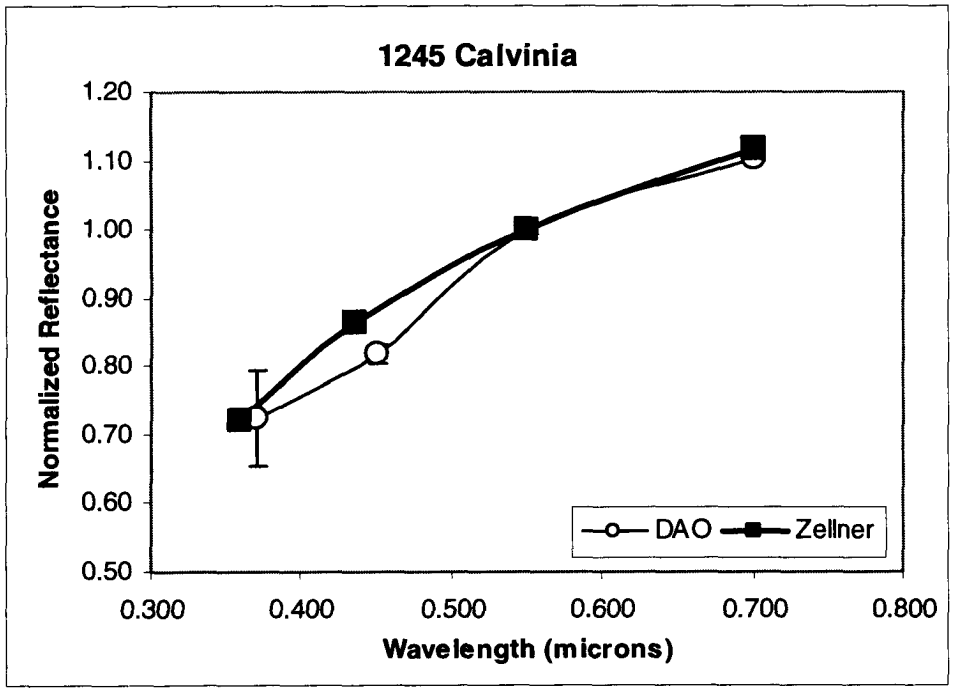

Figure 4.1 cont'd: Reflectance curve for Koronis family asteroids observed at DAO.

e)

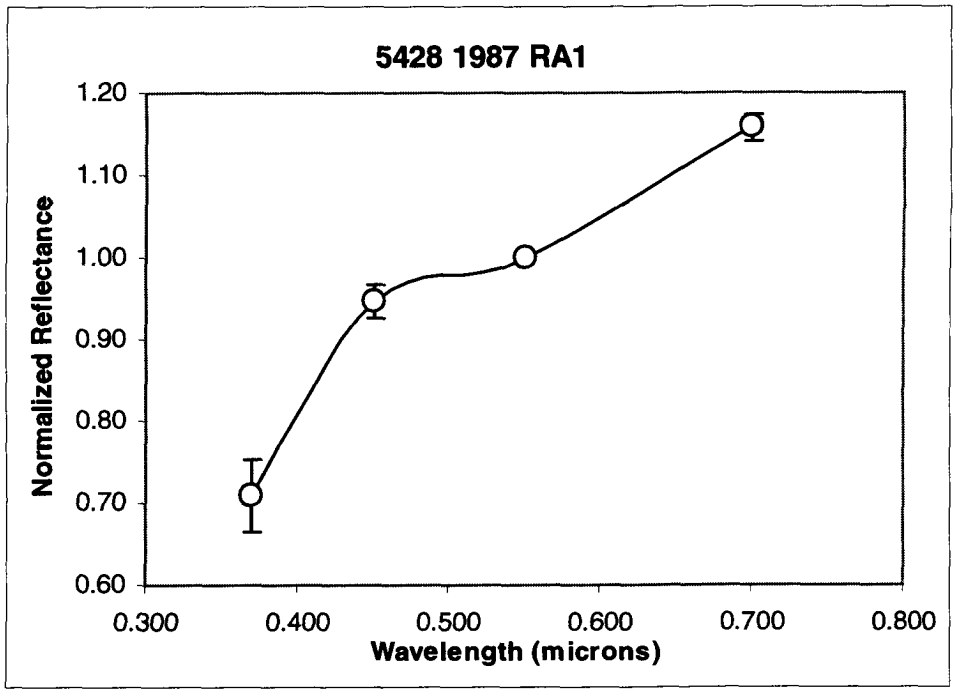

f)

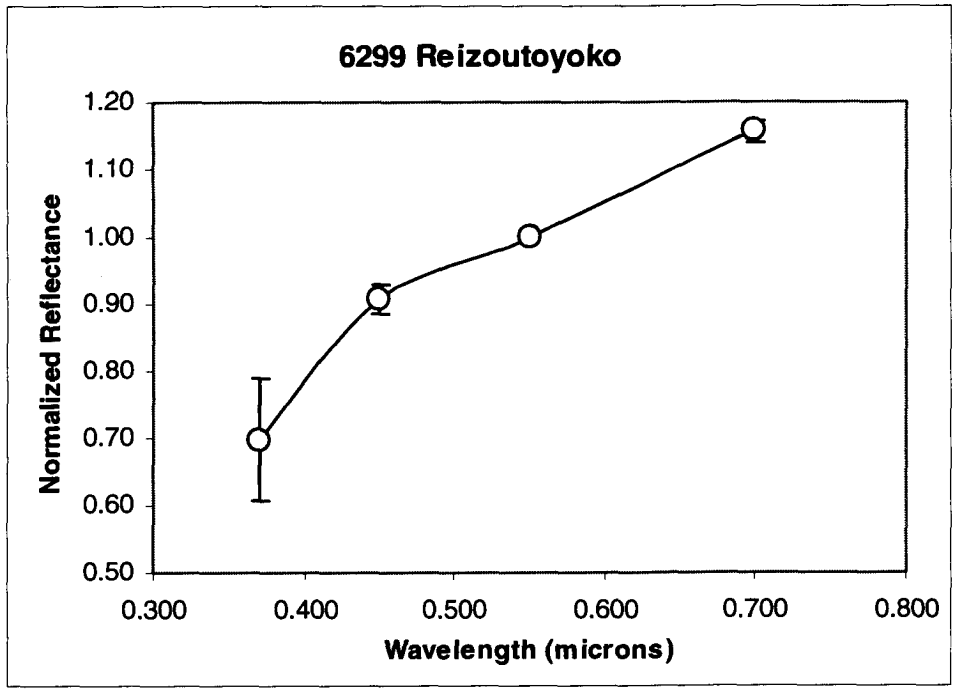

Figure 4.1 cont'd: Reflectance curve for Koronis family asteroids observed at DAO.

g)

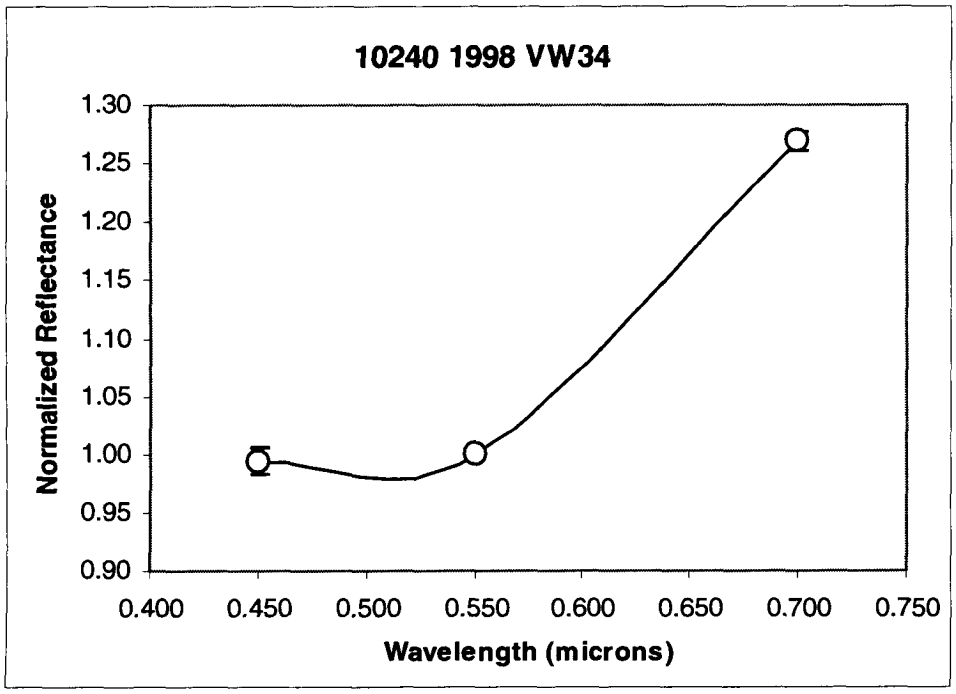

h)

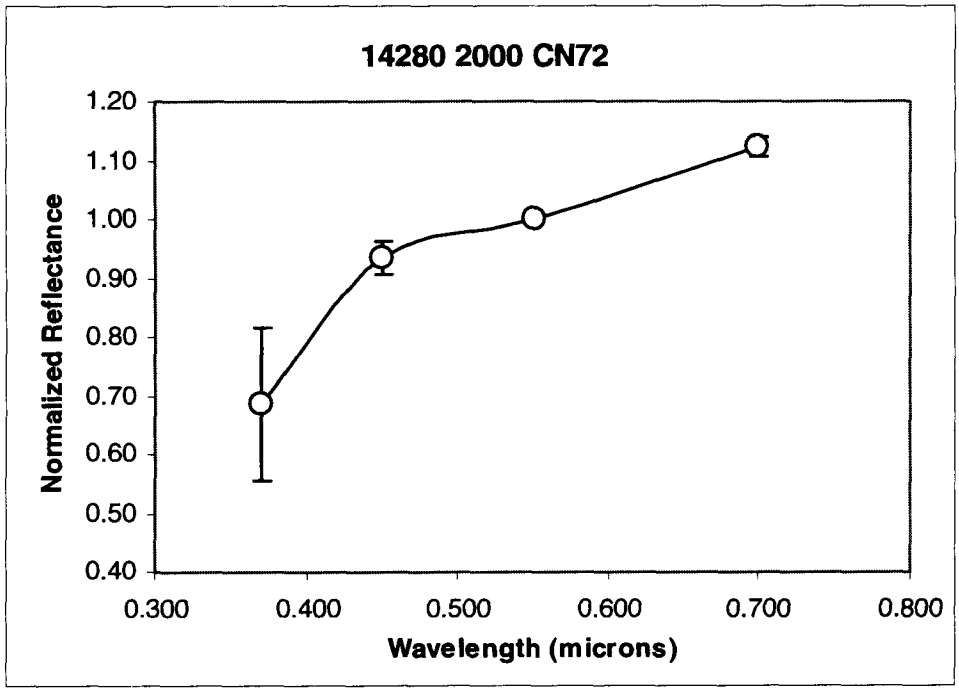

Figure 4.1 cont'd: Reflectance curve for Koronis family asteroids observed at DAO.

i)

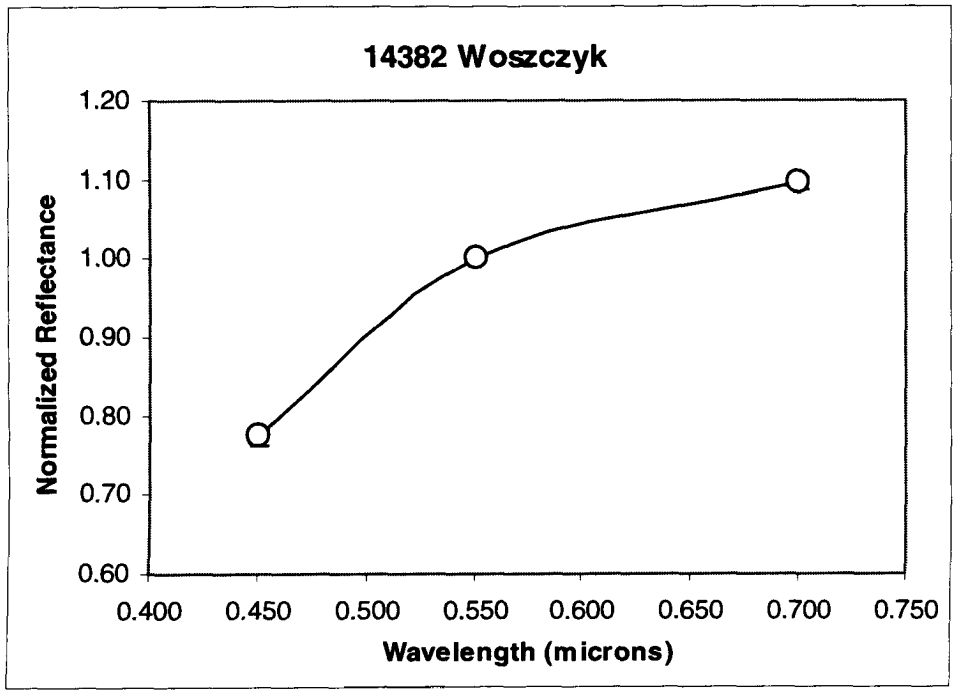

Figure 4.1 cont'd: Reflectance curve for Koronis family asteroids observed at DAO.

a)

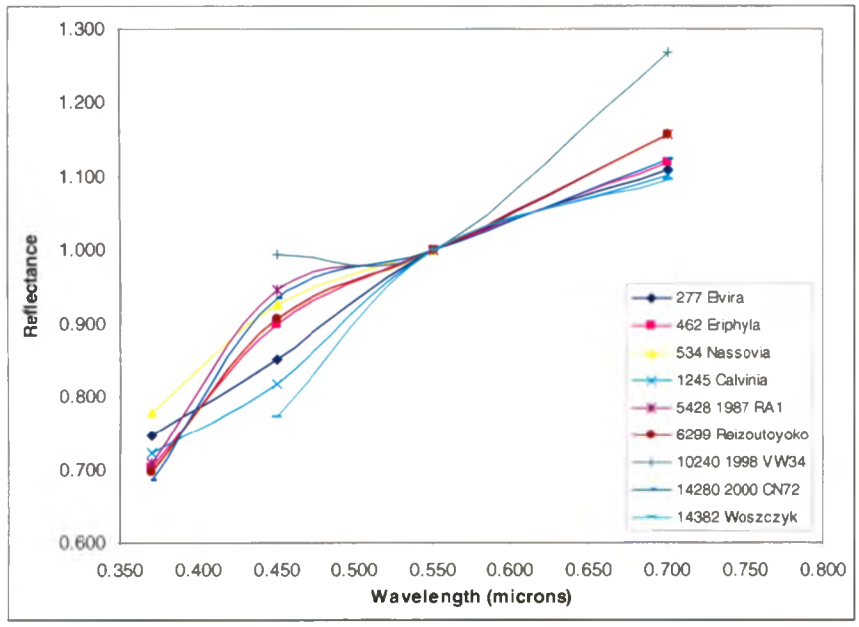

b)

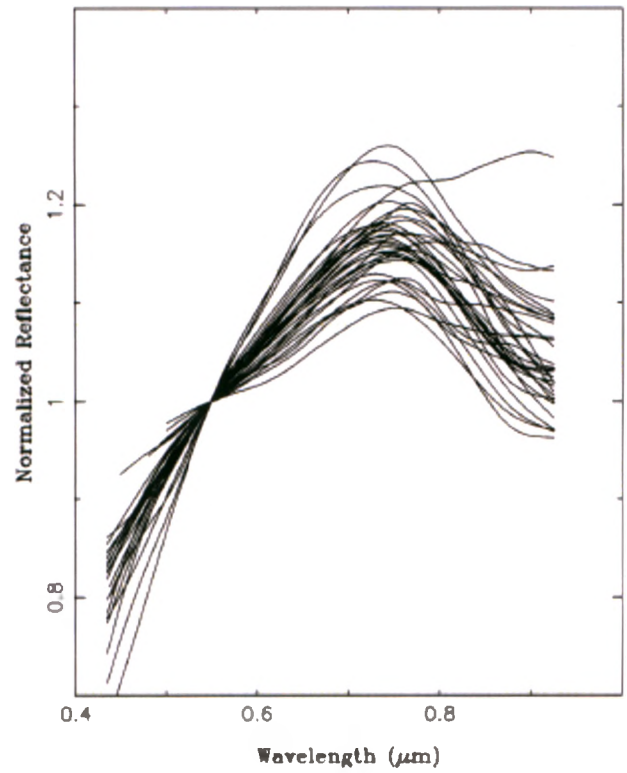

Figure 4.2: a) Reflectance curves for Koronis asteroids observed at DAO, normalized to 1.000 at 0.550 μm. b) Published reflectance curves for Koronis family members, normalized to 1.0 at 0.55 μm (Mothé-Diniz et al. 2005).

Chapter 5

Results and Discussion

5.1 Koronis Family Inflections

5.1.1. Qualitative Analysis of Reflectance Curves

Following Hiroi et al. (2006), the reflectance curve of each target was normalized to unity in the w-band to see if the inflections at 0.42 μm and 0.55 μm were present (Fig. 5.1). Asteroid (534) Nassovia was excluded in this step due to the lack of w filter data. Recall that as the degree of space weathering on an asteroid's surface increases, the inflections at these wavelengths should change towards zero (i.e. C_b and C_v increase). None of the DAO targets appear to show an inflection at 0.55 μm, implying that at 2.5 Gy old, the Koronis family has experienced sufficient weathering to have removed this feature from the spectra of its members. Recent SDSS data for the Iannini family, estimated to be ~3 My old, seems to show the inflection for some but not all members (Willman, personal communication. See also Willman et al. 2008 for Iannini spectra). If these inflections are actually present and are disappearing over a roughly 3 My time scale, the lack of 0.55 μm inflections in Koronis spectra is consistent with expectations. It would also be consistent with weathering timescale estimates from the literature (discussed in chapter 2). Future observations of Karin cluster members at these wavelengths will be useful in putting better constraints on this feature.

Based on visual inspection of the reflectance curves, there is a 0.42 μm inflection for some DAO targets: (5428) 1987 RA1, (6299) Reizoutoyoko, (10240)

1998 VW34, (14280) 2000 CN72, and possibly a weak inflection in the spectrum of (462) Eriphyla. Spectra of Koronis members observed by Zellner et al. (1985b) show no inflections at either 0.42 μm or 0.55 μm, with the possible exceptions of (243) Ida, (761) Brendelia, and (1336) Zeelandia, for which there may be slight inflections at 0.42 μm (Fig. 5.1b).

It should be noted that the Zellner et al. (1985b) asteroids are typically larger than those observed at DAO. Smaller asteroids are statistically younger so it was expected that on average, the smallest and faintest asteroids (i.e. those with the higher asteroid numbers in the legends of Fig. 5.1) would show the strongest features while the brightest and largest did not. The lack of obvious inflections in the Zellner et al. (1985) data is consistent with this though there does not seem to be such a distinct trend in the DAO inflections. Not all small asteroids are young so it may not necessarily be surprising that some do not show the expected inflections. These spectra are somewhat difficult to interpret because the data is not continuous; the curves are interpolations between reflectances in four separate bands. The inflections could imply several things: i) the inflection at 0.42 μm takes longer to be weathered away and, therefore, this region of the spectrum is affected differently by space weathering, ii) the spectral variations may be due to compositional variation among the family members, which may indicate a more complex family structure or possibly multiple parent bodies, or iii) the features may be due to particle size effects.

a)

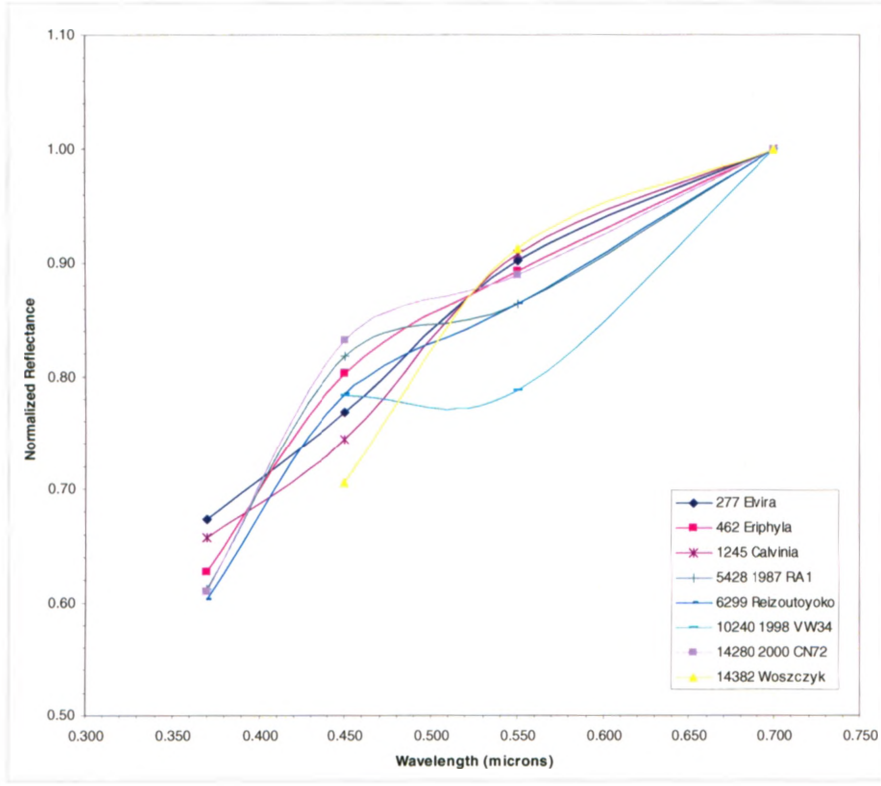

b)

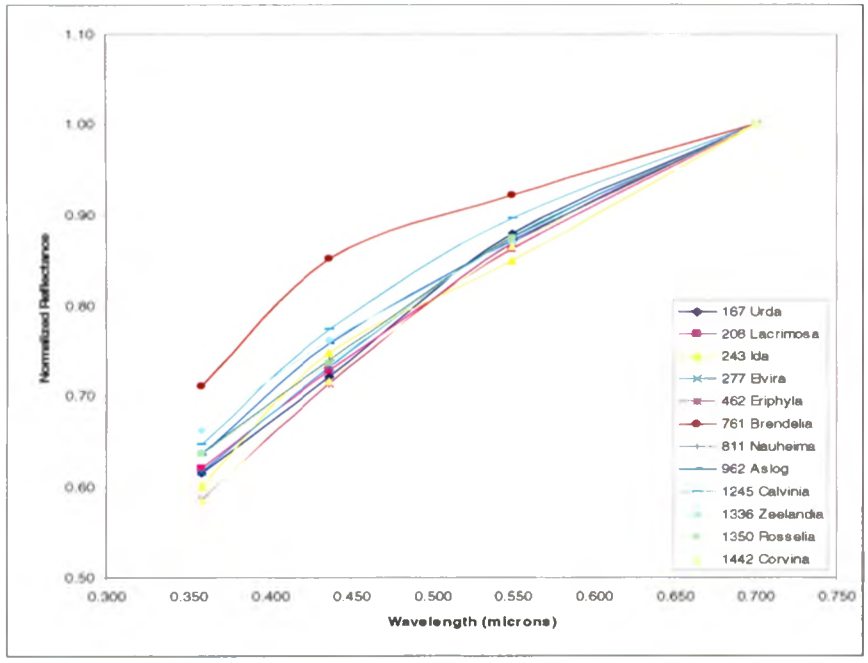

Figure 5.1: Reflectance curves of Koronis members observed a) at DAO and b) by Zellner et al. (1985b), normalized to the w-band. Error bars are excluded for clarity. Typical errors: a) $\delta R_u = 0.043 - 0.172$, $\delta R_b = 0.011 - 0.028$, $\delta R_w = 0.004 - 0.017$. b) $\delta R_u = 0.008 - 0.027$, $\delta R_b = 0.009 - 0.024$, $\delta R_w = 0.007 - 0.034$.

There is evidence that the ultraviolet region of the spectrum, the 0.20 – 0.40 μm range, responds differently to the effects of space weathering. Where spectra are reddened and darkened by weathering effects at visible – near infrared wavelengths, the opposite appears to occur in the UV region. The spectrum becomes brighter at blue wavelengths and studies have shown that the effects of weathering in the UV begin to appear with less weathering than the longer wavelength effects, suggesting that this region is more sensitive to space weathering (Hendrix and Vilas 2006). In some cases, a spectral reversal, where the UV lightcurve is offset by 180° from the visible lightcurve, may also occur (Hendrix et al. 2003). The inflections at 0.42 μm do indicate higher than expected reflectances at blue wavelengths but are not likely to be a manifestation of the effects observed by Hendrix and Vilas (2006). The central wavelength of the ECAS b filter lies just outside of the near-UV range, putting it in the visible portion of the spectrum. In addition, if the UV region is a more sensitive indicator of weathering effects than the longer wavelengths, 0.55 μm inflections should also be present where 0.42 μm inflections are seen. This is not the case in the DAO or Zellner et al. (1985b) observations.

The Koronis family has been noted for its spectral homogeneity but recent work has shown that there may be more diversity among its members than initially believed (e.g. Binzel et al. 1993, Mothé-Diniz et al. 2005). To investigate the possibility of compositional variations, it would be useful to look at the absorption bands near 1μm (a region that was inaccessible with the DAO detector) for each target and look for differences in band depth, band width, and band centre, per Binzel et al. (1993) since all of these properties are affected by changes in

composition. The SMASSII catalogue provides data in the appropriate wavelength region only for asteroids (243) Ida, (462) Eriphyla, and (1336) Zeelandia, all three of which show the 0.42 μm inflection. No spectral data is available for the other targets, making it impossible to draw any conclusions about the compositional variation of these asteroids from the existing observations.

As an alternative means of exploring such variations, Fig. 5.2 shows the heliocentric distribution of the Koronis asteroids observed in both the DAO and Zellner et al. (1985b) datasets, indicating which targets show the 0.42 μm inflection and which do not. Comparing the magnitude of the inflections (by visual inspection of Fig. 5.1) to the distribution of asteroids in proper semimajor axis and proper inclination, the majority of targets for which no inflection is observed have higher inclinations and are located farther from the sun than those which do show the 0.42 μm inflection. The inflections, then, could simply be a function of location within the family, with those members at higher inclinations appearing more weathered than their lower i_p counterparts. If this distribution were to also correlate with spectral differences in the 1μm region, it could be indicative of a compositional gradient, and would lend some support to the idea that the Koronis family was formed from the breakup of two separate bodies with differing mineralogies (Mothé-Diniz et al. 2005). Again, there is not enough data available at present to sufficiently explore this possibility. However, space weathering may not be likely to vary significantly over such a narrow section of the asteroid belt.

The lack of spectral data for these targets also means that particle size effects cannot be conclusively ruled out, since variation in particle size can lead to differences in absorption band depth at 1μm (Binzel et al. 1993).

An additional possibility, inaccurate photometry, is always a concern when observing small, faint objects that are near instrument limitations. As outlined in Chapter 3, all-sky photometry is particularly challenging and highly sensitive to variations in sky conditions. The u filter is the most difficult band in which to obtain reliable values and it can significantly affect the inflection calculations at 0.42 μm. While correctly interpreting the results of this study is complicated by difficulties with the u filter, this is the first dedicated study of this nature and so these observations may at the very least provide a basis for comparison for future studies at more ideal observing locations and with more sensitive detectors.

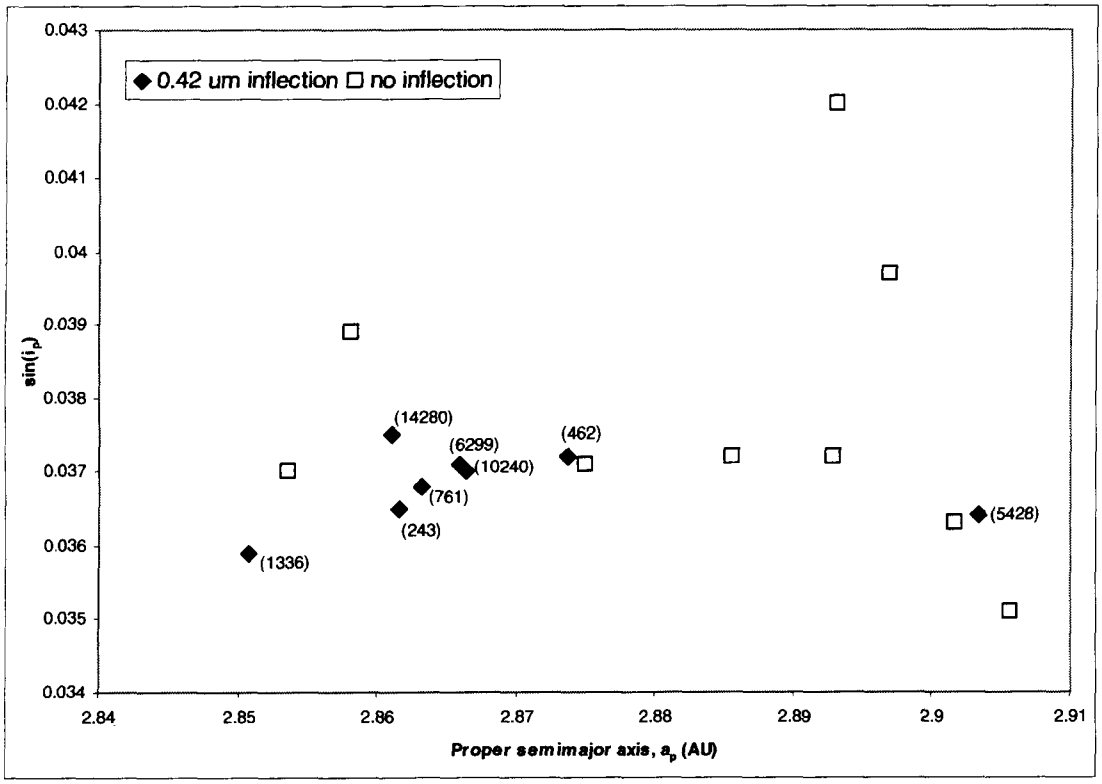

Figure 5.2: Distribution in a_p and i_p of Koronis asteroids observed both at DAO and by Zellner et al. (1985).

5.1.2 Quantitative Analysis of Inflections

The Hiroi et al. (2006) C_b and C_v inflections, calculated using equations 4.8-4.9, are listed in Table 5.1. The C_b values are generally more negative than C_v values, consistent with Hiroi et al.'s (2006) observations, and C_v is clustered around zero for these Koronis members, consistent with the lack of 0.55 μm inflections reported in the previous section (Fig. 5.3a). The errors reported for the C_b inflections are, in most cases, an order of magnitude larger than those for C_v because, as discussed earlier, the u filter is particularly sensitive to variations in atmospheric conditions and the R_u terms had the highest errors, which propagated into the inflections.

Table 5.2 lists C_b and C_v for the Zellner et al. (1985b) targets in the Koronis zone. The values are clustered near zero, even more so than the DAO values (Fig. 5.3b). Note that for the Zellner et al. (1985b) dataset, errors in C_v are comparable to those for the DAO data while the C_b errors are much lower. Where there is overlap between datasets, not all values agree within the error bounds. However, overall trends are quite similar. Differences in instrumentation and technique, as well as large differences in sky conditions all contribute to variations between datasets. It is possible that the differences may be due, in part, to phase angle effects but there is not enough data to determine whether this is the case (see section 5.1.2.4).

Target	**$C_b \pm \delta C_b$ (μm^{-1})**	**$C_v \pm \delta C_v$ (μm^{-1})**
277 Elvira	0.178	-0.688
	± 2.240	± 0.277
462 Eriphyla	-1.440	-0.187
	± 1.144	± 0.134
534 Nassovia	-1.143	-
	± 1.242	
1245 Calvinia	0.610	-1.032
	± 0.930	± 0.130
5428 1987 RA1	-2.445	0.452
	± 0.701	± 0.193
6299 Reizoutoyoko	-1.718	0.109
	± 1.232	± 0.203
10240 1998 VW34	-	1.366
		± 0.093
14280 2000 CN72	-2.463	0.157
	± 1.747	± 0.257
14382 Woszczyk	-	-1.495
		± 0.113

Table 5.1: Summary of inflection values for DAO Koronis asteroids.

Target	$C_b \pm \delta C_b$ (μm^{-1})	$C_v \pm \delta C_v$ (μm^{-1})
167 Urda	0.024	-0.590
	± 0.420	± 0.130
208 Lacrimosa	-0.214	-0.277
	± 0.427	± 0.118
243 Ida	-1.166	0.105
	± 0.216	± 0.112
277 Elvira	-0.249	-0.433
	± 0.367	± 0.223
462 Eriphyla	-0.301	-0.492
	± 0.420	± 0.120
761 Brendelia	-1.264	-0.113
	± 0.416	± 0.269
811 Nauheima	-0.112	-0.373
	± 0.480	± 0.208
962 Aslog	-0.677	-0.134
	± 0.365	± 0.158
1245 Calvinia	-0.615	-0.386
	± 0.278	± 0.148
1336 Zeelandia	-0.393	-0.059
	± 0.406	± 0.220
1350 Rosselia	-0.078	-0.378
	± 0.519	± 0.146
1442 Corvina	-0.433	-0.401
	± 0.673	± 0.235

Table 5.2: Summary of inflection values for Zellner et al. (1985b) Koronis zone asteroids.

a)

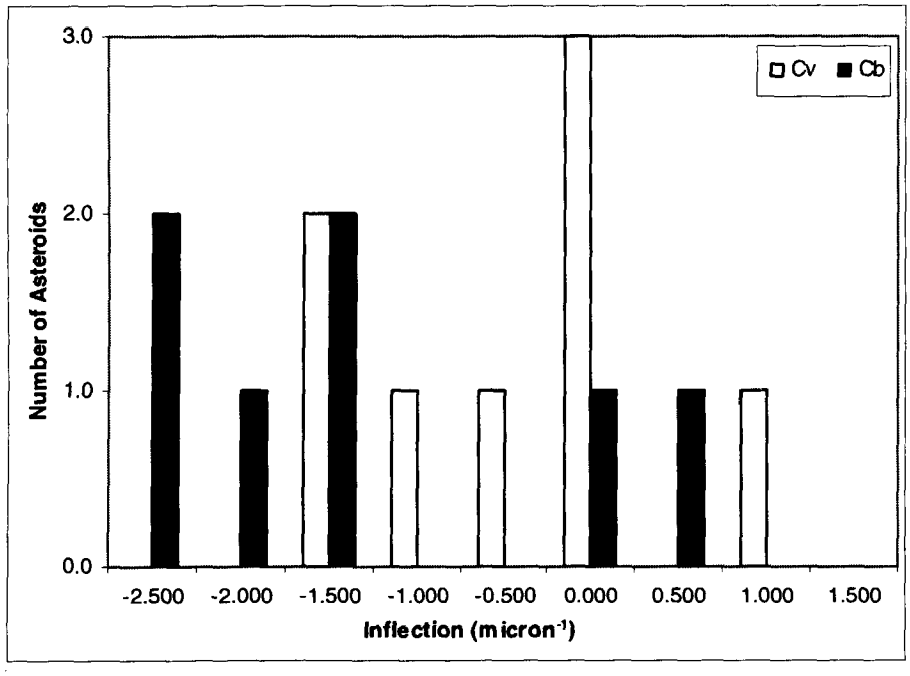

b)

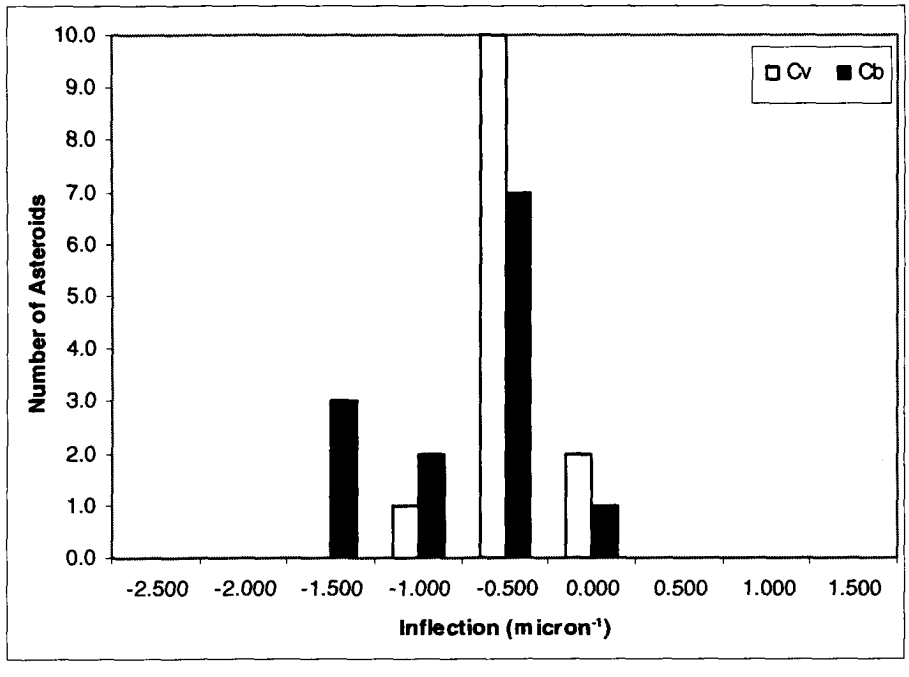

Figure 5.3: Histogram of C_b and C_v calculated for a) DAO targets, b) Zellner et al. (1985b) Koronis zone targets.

5.1.2.1 Variation with Surface Age

Although the formation age of the Koronis family is known and it is assumed that the surface age of each family member was "reset" at the time of formation, it is also very likely that the surfaces of these bodies have been modified over the 2.5 Gy lifetime of the family and that they have not all been modified in the same way (Jedicke et al. 2004).

One common proxy for a body's surface age is its spectral slope, which should become steeper as the body ages (Marchi et al. 2006). In order to determine if these inflections can truly measure the degree of weathering on a surface, they need to be compared to a suitable proxy for the surface age (i.e. a maturity index). Slopes were initially found by fitting straight lines to the Koronis asteroid spectra but were not used in this analysis since it is difficult to fit a straight line to a non-linear curve and the values were not reliable. Instead, the ratio of w-band reflectance to b-band reflectance, R_w/R_b, was used as a maturity index, per Ishiguro et al. (2007). The ratio should increase with increasing surface age, indicating a redder (and thus steeper) spectral slope.

Based on the Hiroi et al. (2006) and Ishiguro et al. (2007) results, it was expected that both C_v and C_b would increase or change towards zero with increasing R_w/R_b, since both should be a signature of increased degrees of weathering. This was the trend seen for C_b but C_v decreased with increasing R_w/R_b for the DAO Koronis asteroids (Fig. 5.4). Both trends have strong correlation coefficients, $r_v = 0.72$ and $r_b = 0.94$. The Zellner et al. (1985b) data produced similar trends, though with more scatter in data points (Fig. 5.5).

Since the ratio R_w/R_b is effectively a measure of spectral slope, it may not be unreasonable for C_v to decrease with increasing R_w/R_b. Looking at the effects of each inflection on the overall reflectance curve (Fig. 1.3), as the C_b inflection becomes smoother, the slope of the curve becomes steeper. On the other hand, as the C_v inflection becomes smoother (while the rest of the spectrum remains unchanged), the slope of the curve becomes shallower. Thus, the trends seen in both the DAO and Zellner et al. (1985b) data are consistent with what would be expected if the inflections are treated as separate features, which are modified at different rates instead of simultaneously.

This may be an indication of a limitation to using Hiroi et al.'s (2006) method for bodies in space, where the exact amount of weathering on a body cannot be controlled or accurately measured as it can in the lab. It is reassuring, however, that despite their opposite trends, both C_v and C_b show a reddening slope.

In contrast, the only other asteroid for which these inflections have been determined, (25143) Itokawa, shows the opposite correlation between C_v and R_w/R_b (Ishiguro et al. 2007). Note, however, that the Ishiguro et al. (2007) trend is based on measurements of a single target while the Zellner et al. (1985b) data for a dozen Koronis asteroids also shows the trends present in the DAO observations.

a)

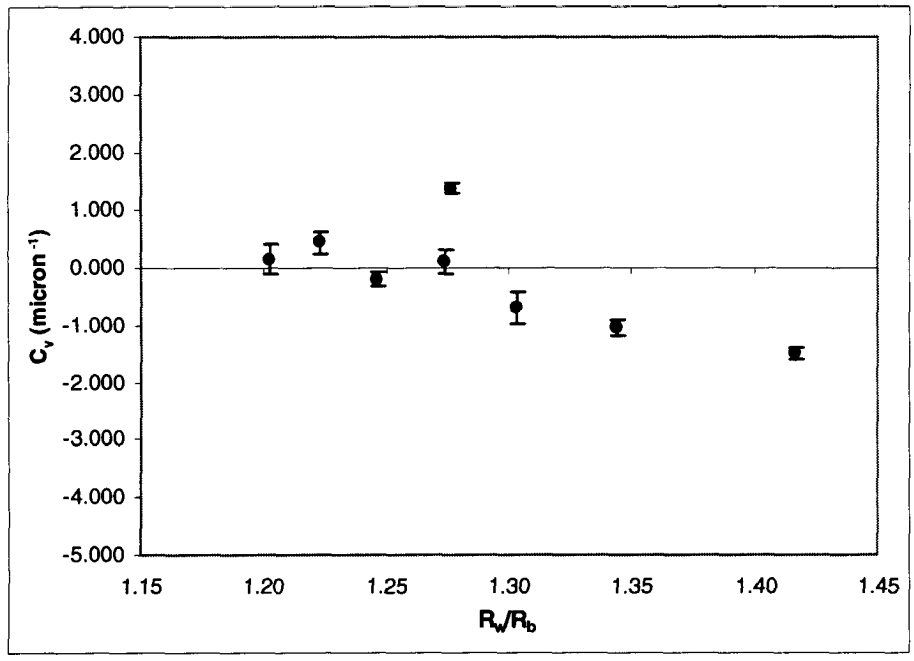

b)

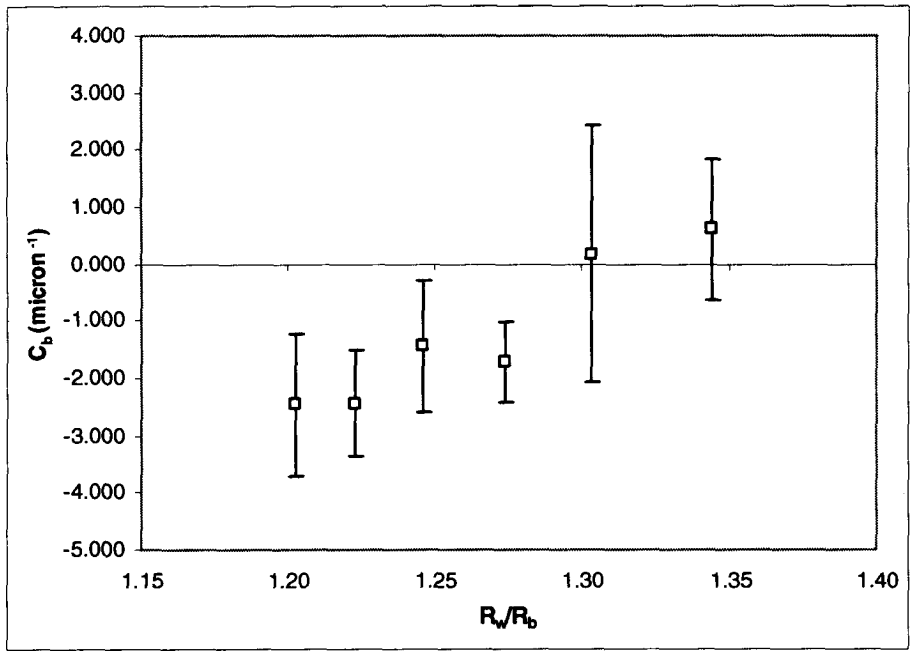

Figure 5.4: The a) 0.55 μm and b) 0.42 μm inflections vs. R_w/R_b for Koronis asteroids observed at DAO.

a)

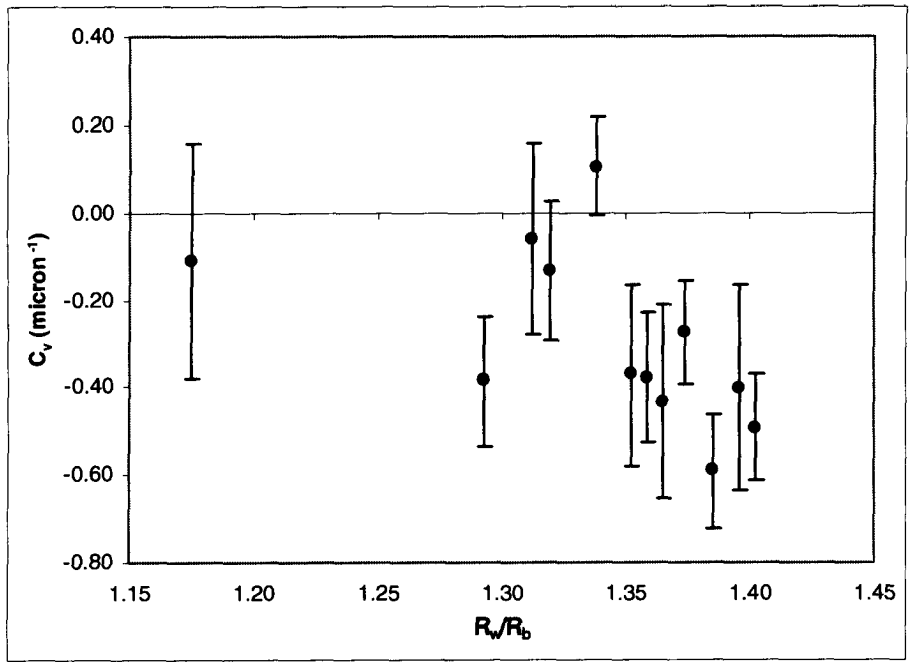

b)

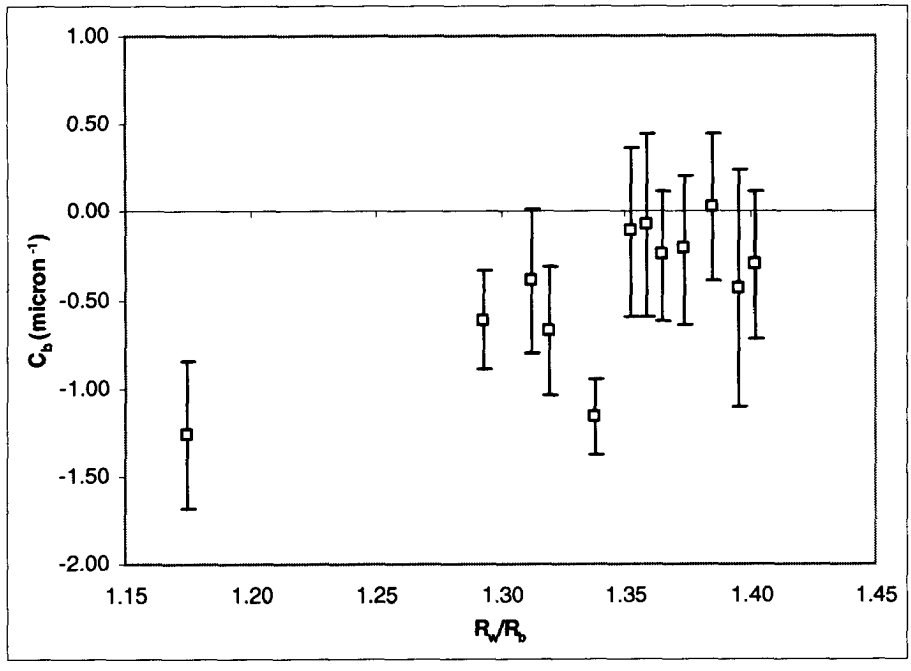

Figure 5.5: The a) 0.55 μm and b) 0.42 μm inflections vs. R_w/R_b for asteroids in the Zellner et al. (1985b) Koronis zone.

5.1.2.2 Variation with Size

There has been conflicting evidence in the literature with regard to size dependent space weathering effects (as discussed in Chapter 2) though the general consensus is that there is no significant relationship between spectral slope and body size for the Main Belt S population (Clark et al. 2002). Past studies focusing on S-type asteroid families, including Koronis and Karin, have found no statistically significant correlation between size and spectral slope (Nesvorný et al. 2005b). To investigate the relationship between the inflections and asteroid size, C_v and C_b were plotted against absolute magnitude, H, a function of diameter, in Figures 5.6 and 5.7.

For the DAO data set, there is a positive correlation between C_v and H, while C_b shows a negative trend (Fig. 5.6). The lack of data points between H = 10.00 and H = 12.50 makes it difficult to gauge the reliability of these trends since the two clusters of data points, if considered separately, show different correlations. The group of points clustered around H = 9.50 show the opposite trends to those observed for the entire set and the points clustered around H = 13.00 have negative trends in both C_v and C_b. It not likely that the trend in C_v is statistically significant (r_v = 0.32) but despite large errors in the C_b terms, the correlation is fairly good, r_b = 0.73. The Zellner et al. (1985b) data set shows overall trends in the same direction as the DAO set, though they are weaker (Fig. 5.7). There is a large amount of scatter in both data sets, which is more obvious in the Zellner et al. (1985) results since they sample a more continuous range of H from H = 9.00 to H = 12.00. These results confirm previous reports that there is no strong relationship between the size of an asteroid and the degree of weathering on its surface.

a)

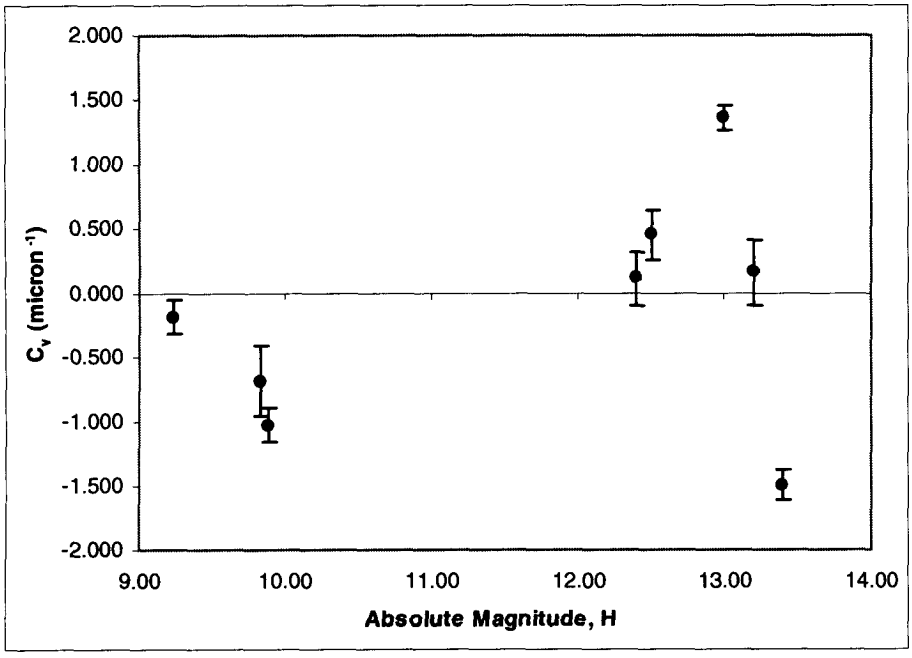

b)

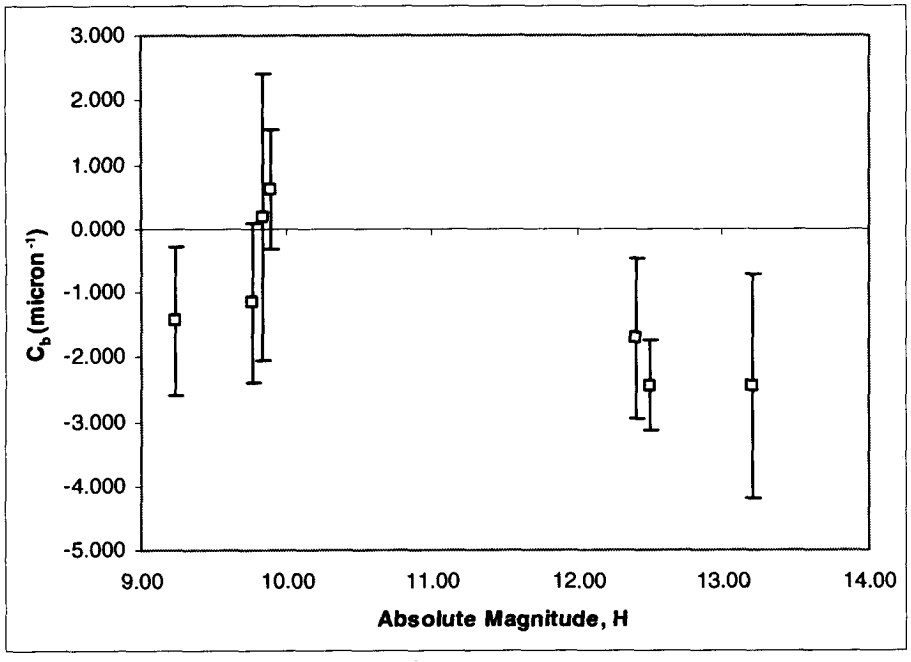

Figure 5.6: Relationship between inflections and absolute magnitude (i.e. size) for DAO targets.

a)

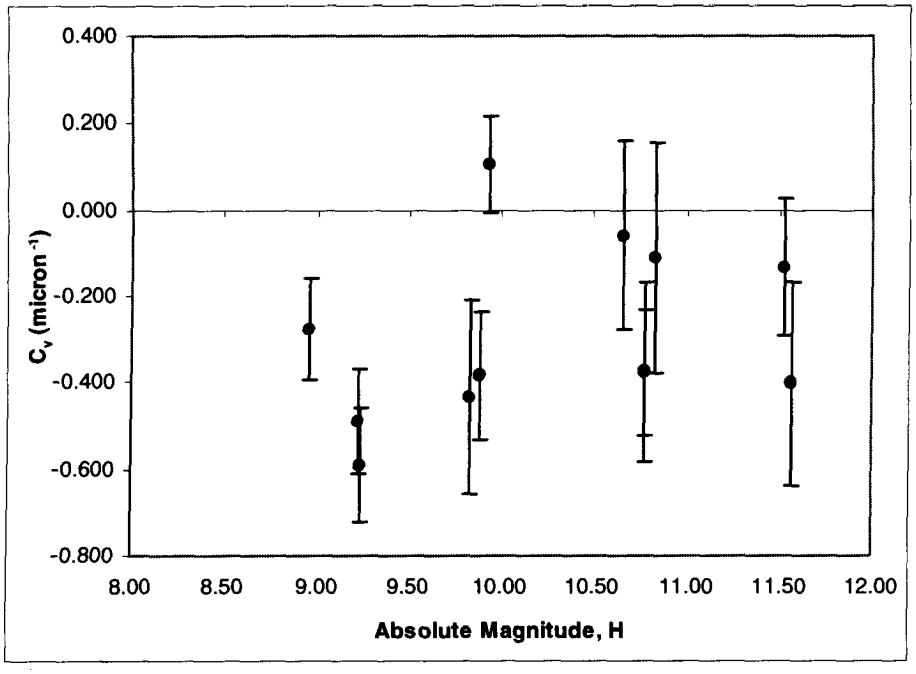

b)

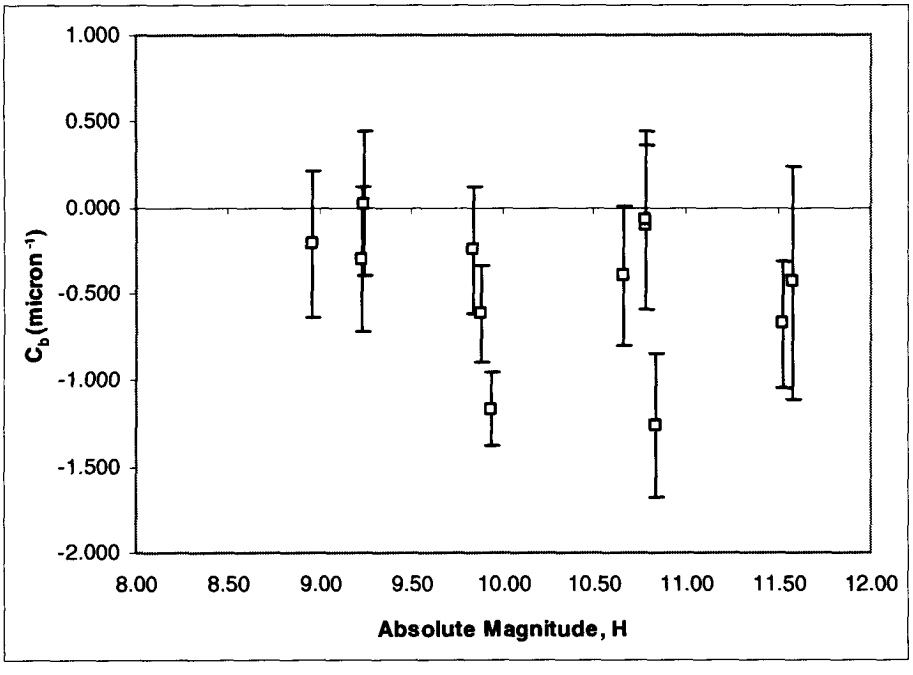

Figure 5.7: Relationship between inflections and absolute magnitude (i.e. size) for Zellner et al. (1985b) Koronis zone targets.

5.1.2.3 Variation with Location in Proper Orbital Element Space

Recent work indicates that space weathering effects have some degree of dependence on distance from the sun (Brunetto and Strazzulla 2005; Marchi et al. 2006), though Nesvorný et al. (2005b) found no statistically significant relationship between spectral slope and distance from the sun in their principal component analysis of SDSS data.

The DAO observations appear to be consistent with Brunetto and Strazzulla (2005) and Marchi et al. (2006); both inflections show a trend with proper semimajor axis (Fig. 5.8). In this case, C_v behaves as expected, indicating less weathering with increasing distance from the sun, while C_b trends in the opposite direction. However, correlation coefficients for both are poor, $r_v = 0.56$, $r_b = 0.32$. There do not appear to be any clear trends for either inflection with proper eccentricity or proper inclination (Fig. 5.10, 5.12); there is too much scatter in data points and the error bars on C_b are too large to be able to identify significant correlations. There is less scatter in the Zellner et al. (1985b) data, but trends are generally flat (Fig. 5.9, 5.11, 5.13). The correlations seen in the DAO data with proper semimajor axis are not reproduced in the Zellner et al. (1985b) set.

While the DAO observations may agree with previous results (with respect to proper semimajor axis), no definitive conclusions can be drawn due to the scatter and large errors. It is also likely that the range in proper orbital elements sampled in this study is too narrow to reveal any significant correlations. Section 5.2 will discuss potential trends for a broader population.

a)

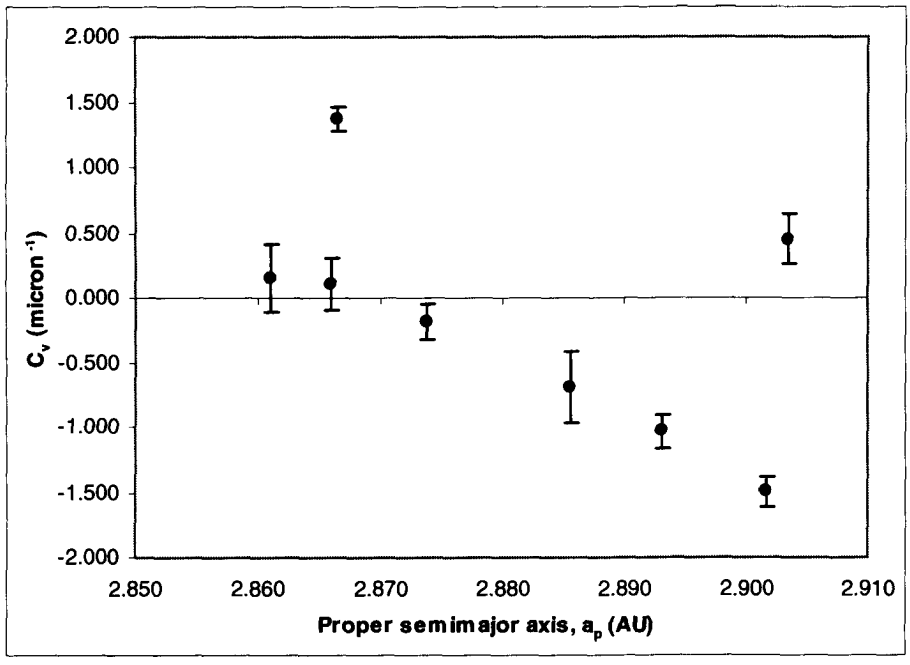

b)

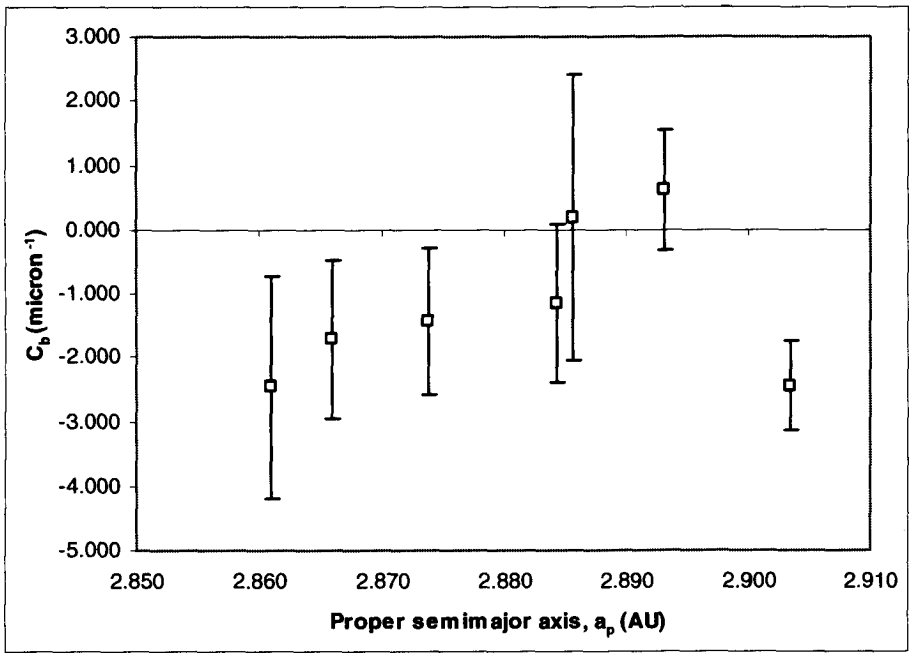

Figure 5.8: Relationship between inflections and proper semimajor axis, DAO targets.

a)

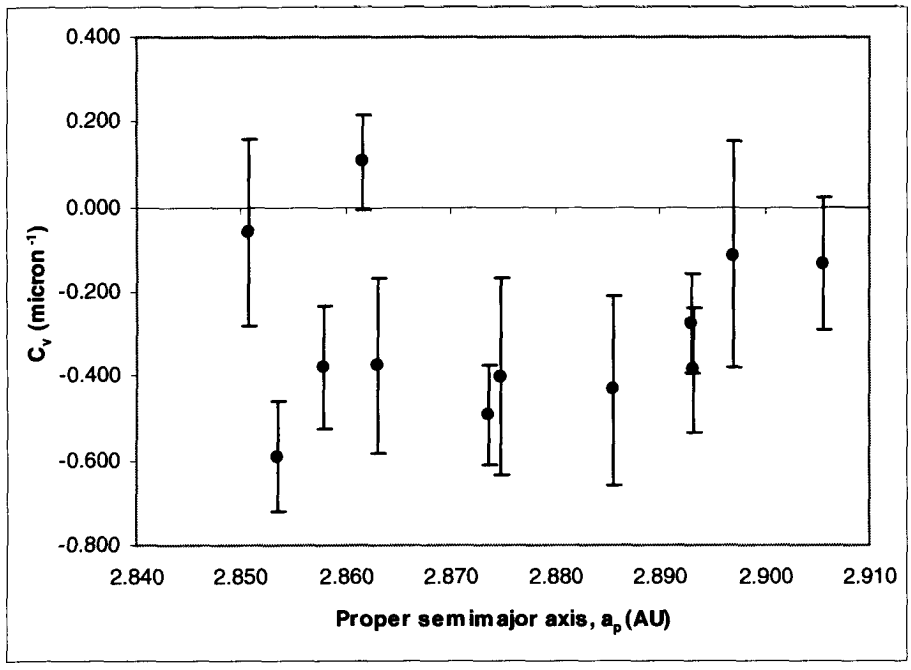

b)

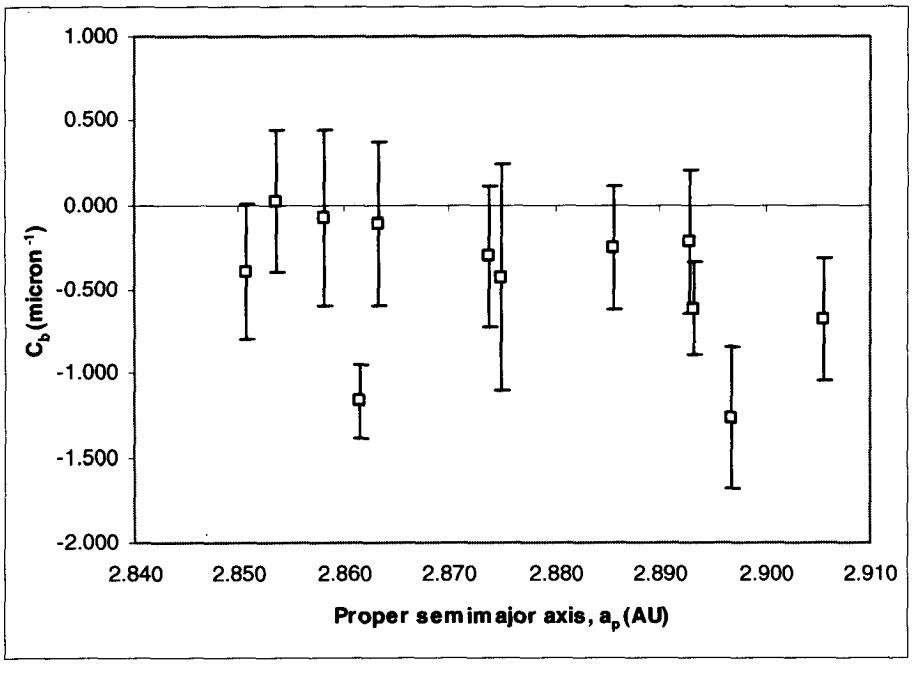

Figure 5.9: Relationship between inflections and proper orbital elements, Zellner et al. (1985b) Koronis zone.

a)

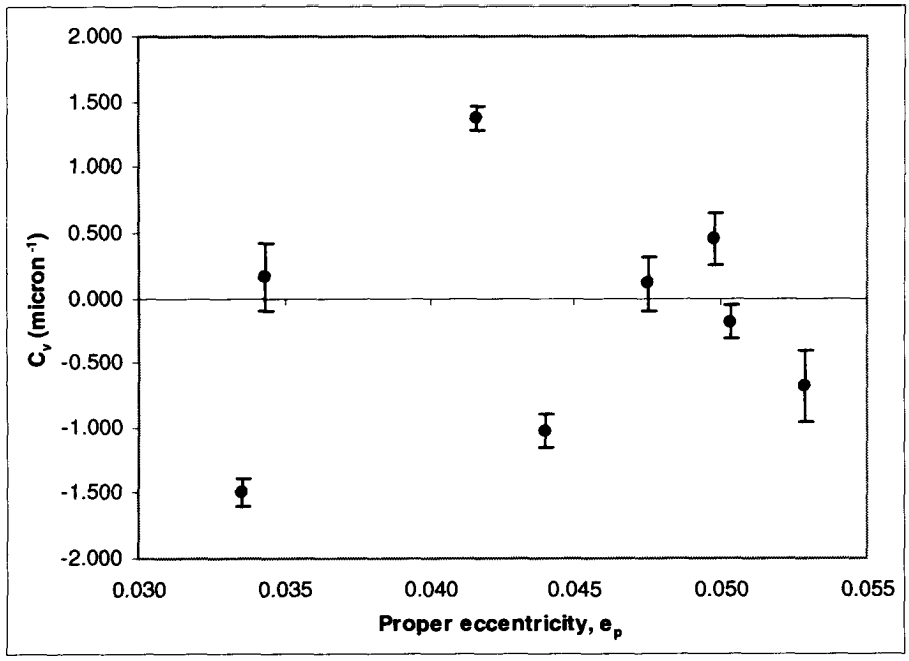

b)

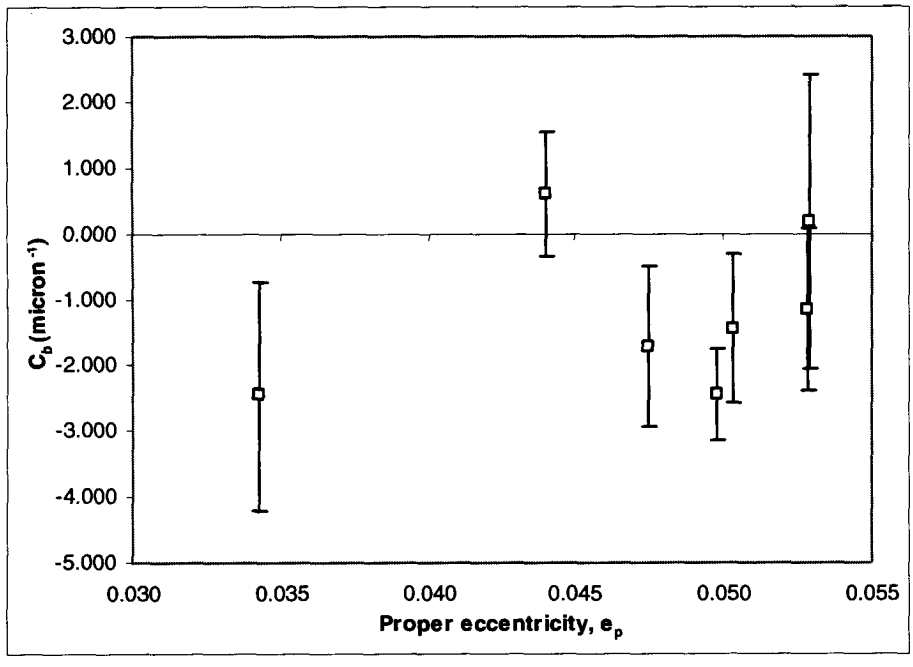

Figure 5.10: Relationship between inflections and proper eccentricity for DAO targets

a)

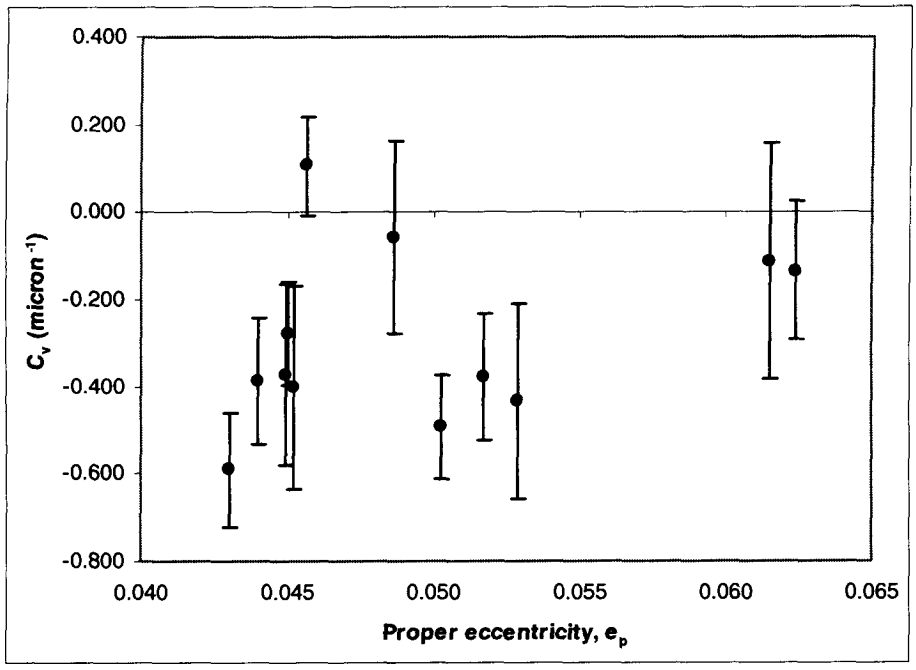

b)

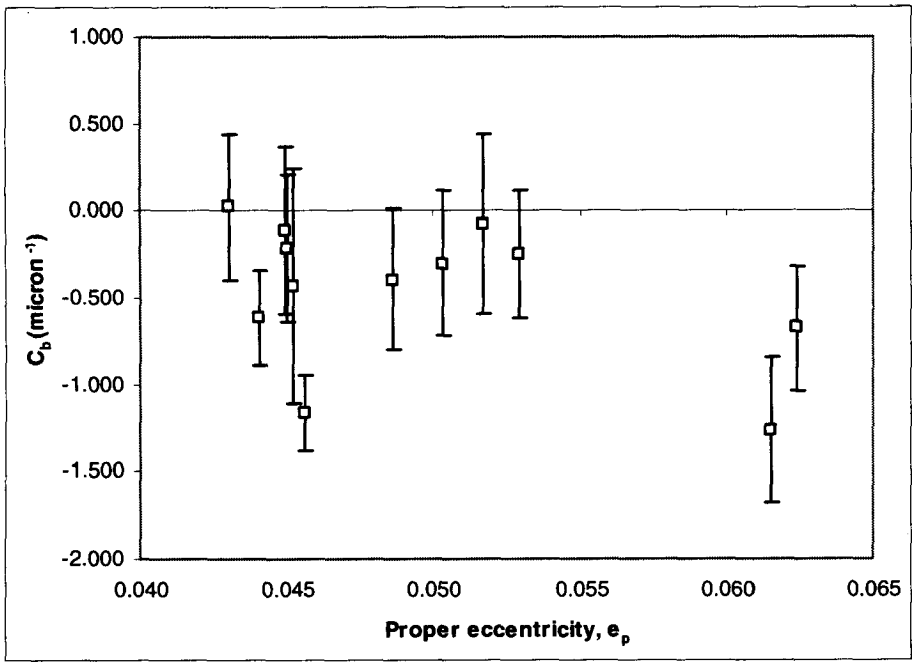

Figure 5.11: Relationship between inflections and proper eccentricity for Zellner et al. (1985b) Koronis zone targets.

a)

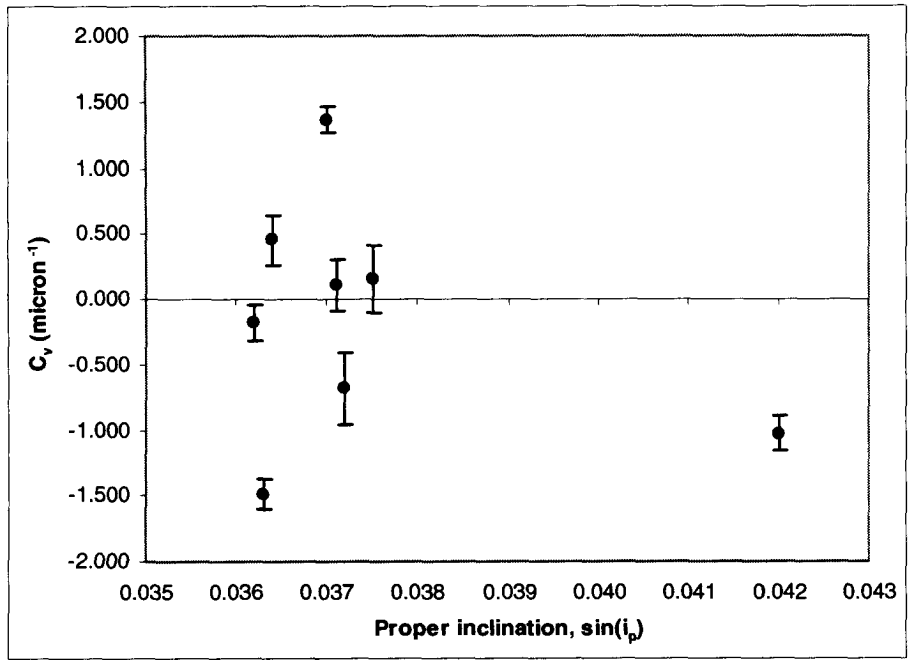

b)

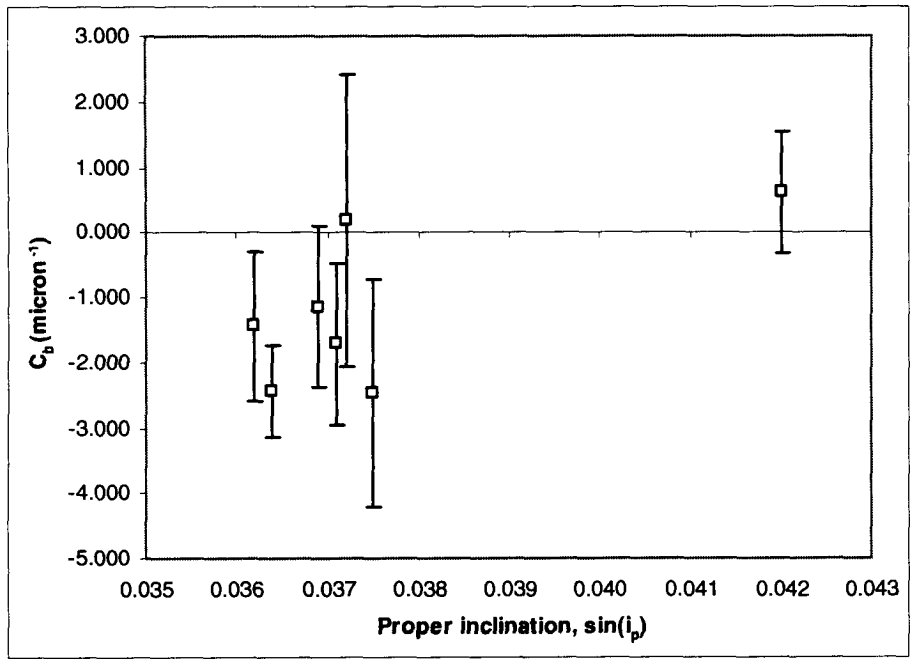

Figure 5.12: Relationship between inflections and proper inclination for DAO targets

a)

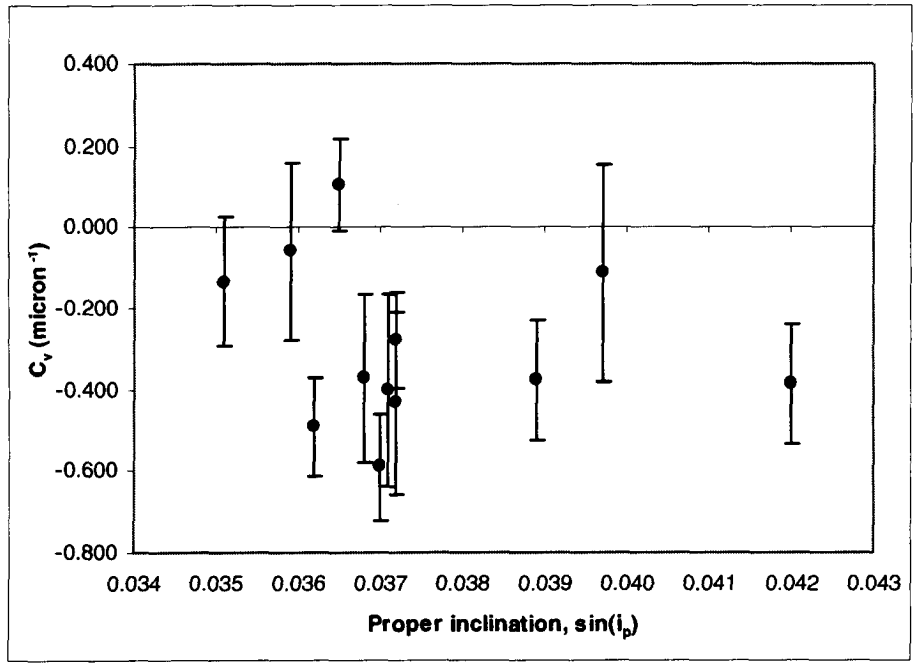

b)

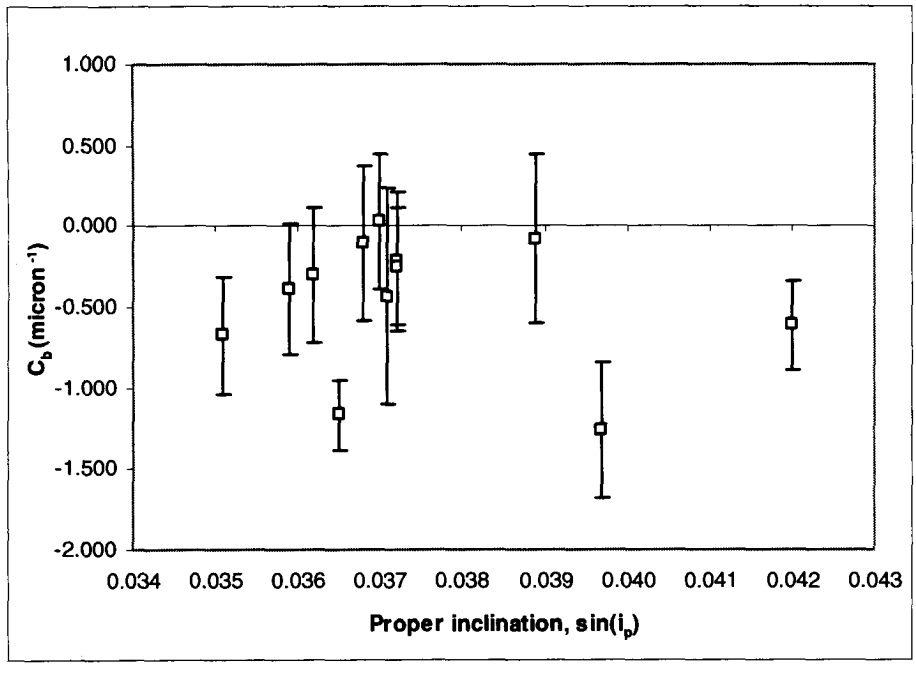

Figure 5.13: Relationship between inflections and proper inclination for Zellner et al. (1985b) Koronis zone targets.

5.1.2.4 Variation with Phase Angle

To confirm Hiroi et al.'s (2006) findings that C_b and C_v do not vary with phase angle, several targets were observed at both DAO and the Elginfield Observatory some months apart. However, since the Elginfield data could not be used, this portion of the study could not be completed.

The three targets that are common between the DAO and Zellner et al. (1985b) datasets were observed at phase angles differing by up to 13.6° (Table 5.3). Only the inflections calculated for (277) Elvira, where the difference in phase angle between datasets is smallest, agree within the error bounds. The lack of agreement for the other two targets cannot be attributed to phase angle differences with any certainty, however. More observations of several targets over a range of phase angles, and under more ideal conditions, are needed to truly confirm or reject the Hiroi et al. (2006) results.

Target	DAO*	Zellner et al. (1985b)
277 Elvira	5.88°	9.35°
462 Eriphyla	8.90°	15.66°
1245 Calvinia	10.02°	-3.57°

*From JPL Horizons ephemeris generator.

Table 5.3: Solar phase angles of targets common to the DAO and Zellner et al. (1985b) datasets.

5.2 Inflections of Other Main-Belt S-type Populations

To investigate how the results described for Koronis members in the previous section compare to the broader Main Belt S population, inflections were found for

the targets in Zellner et al.'s (1985b) S-type orbital zones (Table 3.3). As before, the inflections were plotted against R_w/R_b to see how they may vary with surface maturity (Fig. 5.14). Error bars are excluded in order to keep the plots legible. Three of the orbital zones (Apollo/Amor/Atens, Phocaeas, and Main Belt) are dynamical groups, asteroids clustered in proper orbital element space due to some long-term dynamical process (Carvano et al. 2001). They are not families, so they represent the background S population. The asteroid families are represented by the Flora, Koronis, and Eos zones.

Where it was previously observed that C_v decreased with increasing R_w/R_b for the DAO and Zellner et al. (1985b) Koronis data, this is not the case for the general S population. In fact, there is no distinct trend in either direction. There is, however, some minor clustering of data points for members in the various zones. One could attempt to predict the surface ages of the family members using Fig. 5.14a, assuming that small values of C_v and small R_w/R_b correspond to younger surfaces. One would then expect that Eos asteroids would have the freshest surfaces, followed by Koronis asteroids, then Flora members. Taking into account the actual dynamical ages of these families (Nesvorný et al. 2005b), the correct sequence should be the reverse, though there has been much debate regarding age estimates for Eos (Doressoundiram et al. 1998). Although no obvious negative trends are present, this seems to suggest that C_v does have an inverse relationship with R_w/R_b. If so, this result is consistent with the DAO Koronis results. The other zones, representing the background asteroids, show a large spread in values, as would be expected for a heterogeneous population.

In the DAO Koronis data, C_b increased with increasing R_w/R_b, as expected. That trend is seen in the broader population as well (Fig. 5.14b). Each zone has a positive slope with moderate correlation, $r \approx 0.5$ to 0.7. There is more distinct clustering compared to the C_v plot but if one attempts to estimate surface age, the same sequence results as before: Eos members appear to have the freshest surfaces, then Koronis members, then Flora asteroids. That the reverse sequence is obtained despite C_b behaving as expected is difficult to interpret. It is possible that there is an anticorrelation between slope and surface age proxy. It is also possible, however, that there is too much scatter in the data and the correlation is too weak for both C_b and C_v to determine any conclusive trends.

The relationship between inflections and size is plotted in Fig. 5.15. There are no obvious trends for C_v with absolute magnitude, though it is worth noting that there is much more distinct clustering of the populations now as they each contain asteroids of a particular size range. In the DAO Koronis results, though it was difficult to conclude with any certainty that there was a relationship, there did appear to be a negative correlation between C_b and H. This trend is observed for all of the Zellner et al. (1985b) S-type zones except Eos. However, the slopes are very close to zero and r values are poor, so as before, no definitive conclusions can be drawn regarding size dependence. This suggests that there is no significant dependence, as the literature indicates.

a)

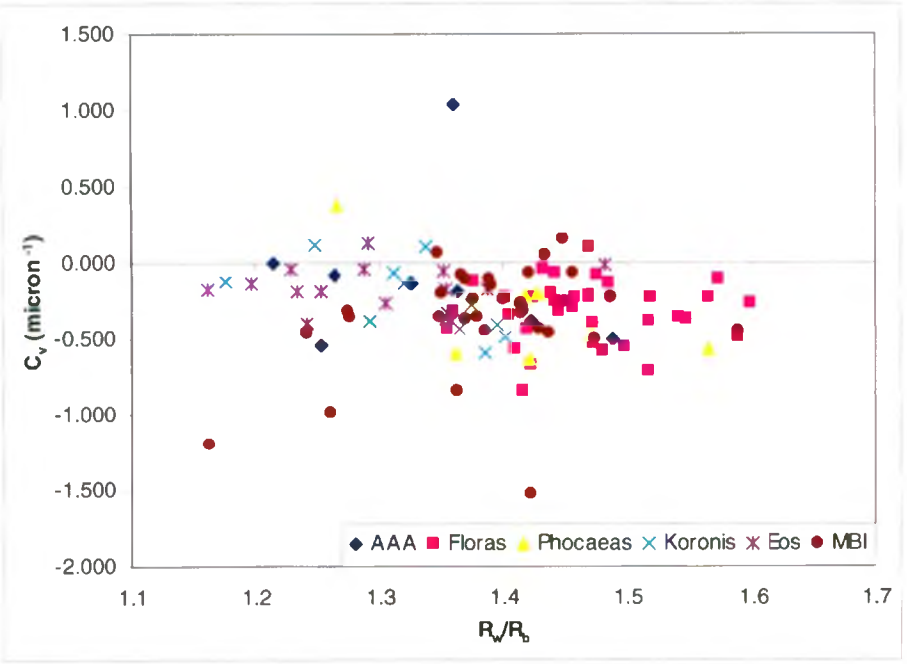

b)

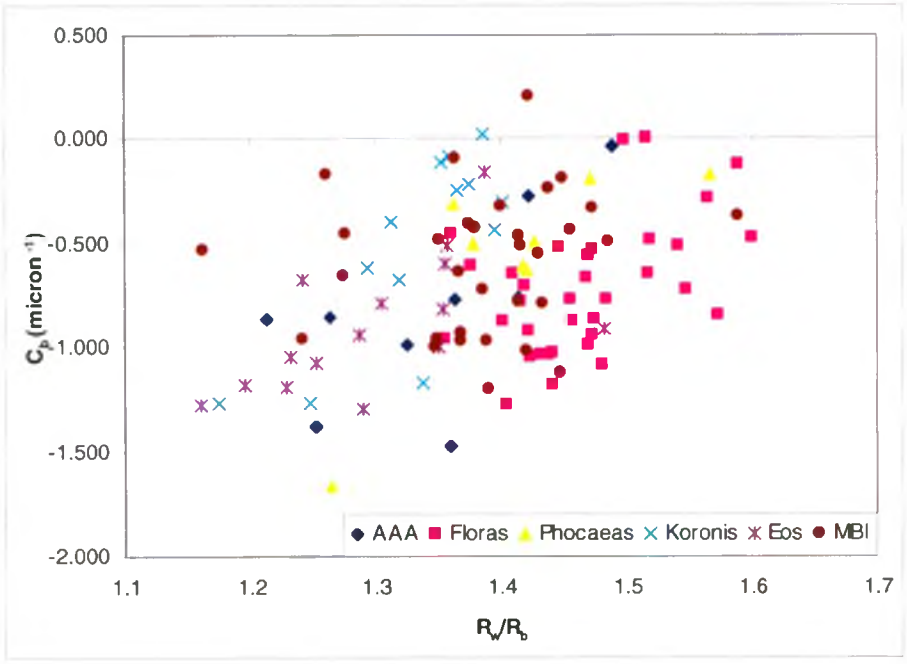

Figure 5.14: Relationship between inflections and R_w/R_b for Zellner et al. (1985b) S-type zones

a)

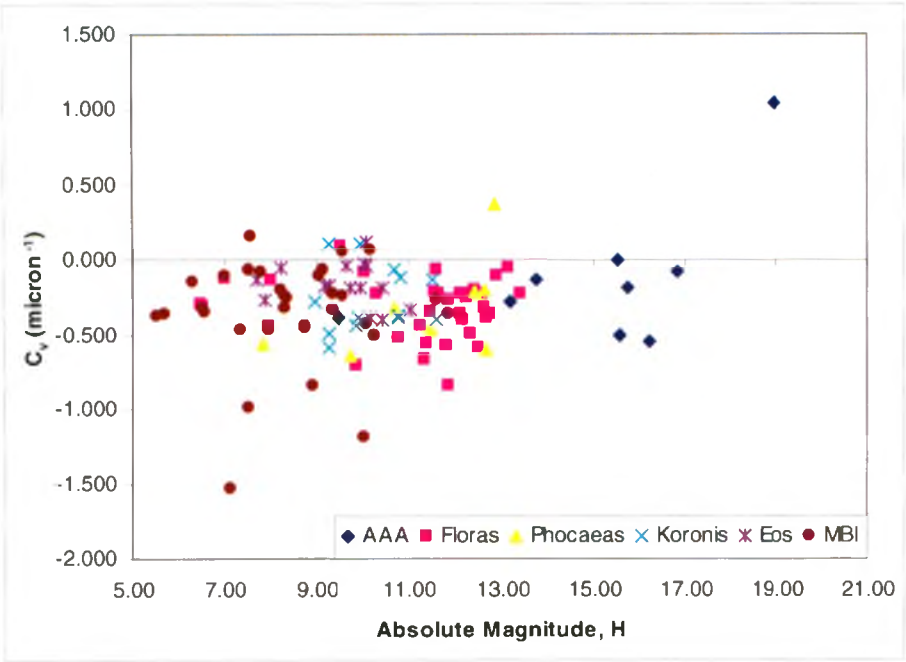

b)

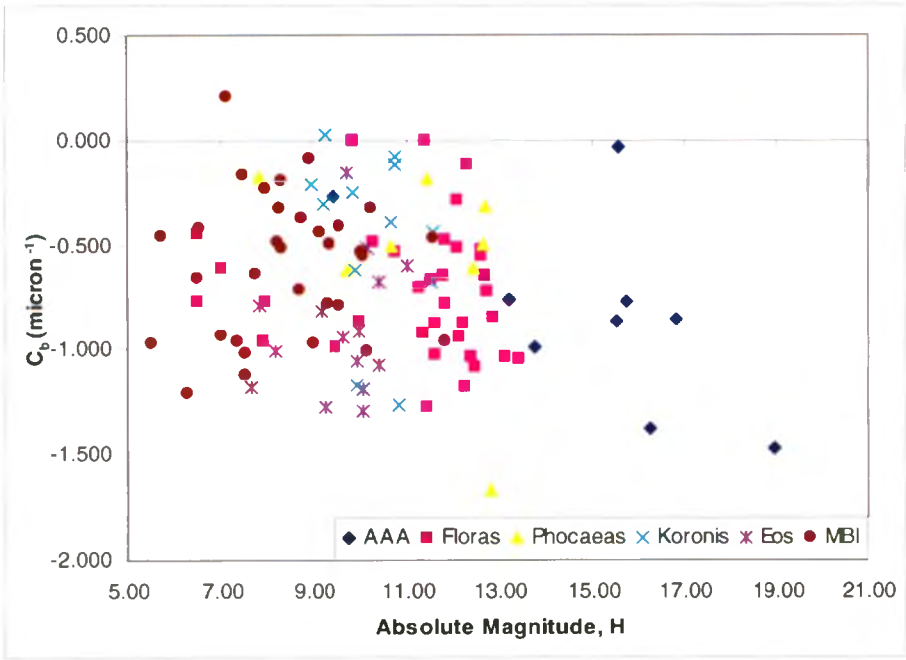

Figure 5.15: Relationship between inflections and absolute magnitude for Zellner et al. (1985b) S-type zones

Proper orbital elements were not available for all of the zones studied, so mean inflections were plotted against osculating semimajor axis to check for correlations (Fig. 5.16). The results agree with the DAO trends up to a ≈ 2.6 AU; the Koronis and Eos mean inflections do not follow the overall trend and the correlation coefficients for both C_v and C_b are very poor (r = 0.04 and r = 0.08, respectively). If the mean inflections for the Koronis and Eos families are removed, the correlations become very strong, r = 0.98 and r = 0.94. This implies that there is a relationship between the degree of weathering on a body and its distance from the sun, though the change near 2.6 AU is suspect. Perhaps there are errors in the dataset for those two families, or something more complex is occurring in the outer Main Belt.

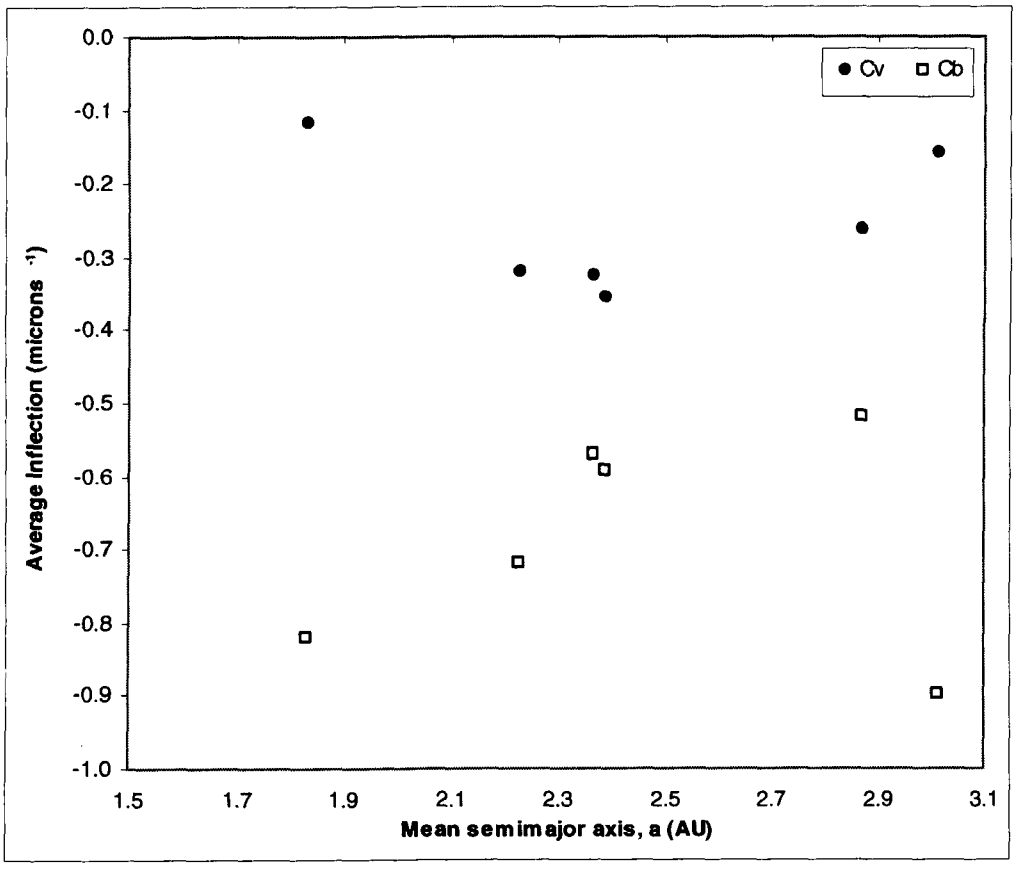

Figure 5.16: Distribution in osculating semimajor axis of mean inflections for each S-type zone in the Zellner et al. (1985b) dataset.

5.3 Space Weathering Timescales

The third objective of this study was to use the Hiroi et al. (2006) inflections, along with the dynamical ages of the families for which data was available, and attempt to put constraints on space weathering timescales. As discussed in Chapter 2, the majority of estimates fall between 10^4 and 10^8 years, depending on the dominant mechanism. It has been discussed in earlier sections that the dynamical age of any asteroid family can only be used as a limiting value. Over their lifetimes, asteroids will be collisionally disturbed on a timescale that is related to their size (known as their "collisional lifetime").

When Binzel et al. (2004) observed the size-dependent transition in spectral slope from Q-type to S-type NEAs, they proposed that the average age of a 5 km asteroid should set the timescale for the weathering process to reach maturation because asteroids > 5 km had nearly constant slopes. Bottke et al. (2005) have modeled the collisional lifetimes of asteroids and found that the interval between km-sized impacts in the near Earth environment is 0.5 My, consistent with the lower range of weathering timescale estimates. Collisional lifetimes do not scale the same way for NEOs as they do in the Main Belt, however, where the lifetime between collisions for a body of comparable size would be somewhat shorter (Bottke et al. 2005).

The average diameter of the larger Koronis members observed at DAO was ~ 30 km. Asteroids of that size are disturbed once every 20 – 25 Myr, while bodies with D ~ 10 km (average size of the smaller targets observed at DAO) are disrupted once every 3 x 10^5 years, or 0.3 My (Bottke et al. 2005). This suggests that over the 2.5 Gyr lifetime of the Koronis family, these asteroids could have been disrupted and had their apparent surface ages reset multiple times. If the lifetime of a 5 km asteroid is the benchmark for space weathering timescales on all asteroids, and assuming that the dynamical age of the Koronis family is the surface age for all of its members, the lack of inflections observed for Koronis members at 0.55 μm is what would be expected for surfaces that are 2.5 Gy old. Taking into account that the asteroids may have been disturbed since the family was formed, weathering on the smallest of observed targets may not yet have reached maturation and inflections

would be expected. In a qualitative sense, the results presented here are broadly consistent with the existing literature.

ECAS Karin spectra would be particularly useful in this context as Karin is much younger than the Koronis family, though recent work by Chapman et al. (2008) showed that while Karin members do appear less red than Koronis members, the differences are very slight. They concluded that weathering of S-types proceeds rapidly, but does not go entirely to completion in several million years, contradicting Binzel et al. (2004).

Mean C_b and C_v were calculated for Koronis, Flora, and Eos members (using the Zellner et al. 1985b results) and were compared to their dynamical ages (Table 5.4). As Table 5.4 indicates, however, it is not possible to compare the inflections of various asteroids and predict which bodies have the most mature surfaces. There are likely numerous factors involved, including surface composition (particularly the olivine/pyroxene ratio) and large uncertainties in the age estimates, all of which make accurate interpretations difficult.

Family	Mean C_b (μm^{-1})	Mean C_v (μm^{-1})	Age (Gy)
Flora	-0.719	-0.321	1.0 ± 0.5
Eos	-0.898	-0.159	2.0 ± 0.5
Koronis	-0.519	-0.263	2.5 ± 1.0

Table 5.4: Mean inflections and dynamical ages for Zellner et al. (1985b) S-type families. Ages are taken from Nesvorný et al (2005b).

Chapter 6

Conclusions and Future Work

6.1 Summary of Results

The purpose of this study was threefold: first, Hiroi et al.'s (2006) new scheme for estimating the degree of weathering on asteroid surfaces using an ECAS system was tested through a survey of Koronis asteroids, in conjunction with the Zellner et al. (1985b) ECAS results. The Zellner et al. (1985b) data set was then used to extend the Koronis family results to a broader population. Third, it was hoped that these results would lead to new constraints on, or a better understanding of, space weathering time scales.

For the Koronis asteroids observed at DAO, the C_b inflection increased with increasing surface maturity, as expected based on Hiroi et al.'s (2006) results, while the opposite trend was observed for C_v. No significant relationship between the degree of weathering and asteroid size was observed for the Koronis family members, though such a relationship cannot be ruled out based solely on these observations. There may be a dependence on proper semimajor axis within the Koronis family, though the two inflection values show slopes in opposite directions and again, the large errors and scatter in data make it difficult to make any definite claims. The range in a_p values was also quite narrow. The fact that C_b and C_v do not trend in the same direction in most cases suggests that the two inflections are independent of each other, i.e. the spectrum in each region may be modified at a different rate or by different means. Though there are many potential explanations, it

is difficult to reliably interpret these observations due to the lack of supplementary data and large photometric errors, particularly in the u-band.

In Hiroi et al.'s (2006) experiments, both C_b and C_v were unaffected by phase angles up to 60°. Phase angle effects could not be tested in this study, so whether or not C_b and C_v are stable against these effects for bodies in space remains unknown.

The Zellner et al. (1985b) dataset was used to extend the Koronis family results to the broader Main Belt and Near Earth S-type asteroid populations. No significant relationship between the inflections and surface age proxy was observed for the general population, consistent with the literature (Clark et al. 2002). As before, no significant size dependence was observed though once again, due to the scatter in the data and large error bars, such a relationship cannot be ruled out. Unlike the DAO Koronis results, there is a distinct relationship between the degree of weathering on a surface and its distance from sun for the general Main Belt S population, though C_b and C_v show trends in opposite directions as before. C_v decreases with increasing heliocentric distance, as would be expected, while C_b increases.

While no significant inflections were observed at 0.55 μm, several targets showed an inflection at 0.42 μm. No Karin members could be observed and consequently, the existing data set was not sufficient for a quantitative analysis of weathering timescales. The lack of 0.55 μm inflections does show, however, that the Koronis family has experienced a sufficient degree weathering to have removed that

feature. Thus it can be concluded that bodies which are 2.5 Gy old would not be likely to show an inflection at 0.55 μm (i.e. $C_v \approx 0$).

In general, the method proposed by Hiroi et al. (2006) showed promising results in the lab. This study has shown, however, that applying it to bodies in space is much more complex. High precision photometry is difficult, particularly the u filter, and all-sky photometry requires exceptional sky conditions. In addition, exact surface composition, age, exposure duration, and weathering process(es) for the bodies being observed cannot be controlled, or even well determined in most cases, making interpretation of the results more challenging.

6.2 Future Work

The methods described here can potentially be very useful in better understanding space weathering processes and estimating the degree of weathering on bodies. To do it successfully, however, a much more rigorous survey over a longer time scale would be required. Ideally, several families spanning a range of dynamical ages should be observed, and with a broad (and continuous) distribution in absolute magnitude. No Karin members were observed for this study, so observations of Karin family members in ECAS would be especially useful for comparison with the results presented here. In addition, several observations of the same targets over a range of phase angles would be needed to determine phase effects on C_b and C_v. Such surveys should be carried out in a location better suited to all-sky photometry and with a detector that is sensitive in both the UV and NIR regions of the spectrum to allow for better, more reliable coverage.

One of the difficulties encountered in this study was a lack of supplementary data when follow-up was needed to examine the likelihood of compositional variations. It is recommended that future studies of this type aim to select targets for which IR data is available, in the SMASSII catalogue or elsewhere, in order to better explore the potential implications of the results.

Bibliography

Abe S., Mukai, T., Hirata, N., Barnouin-Jha, O. S., Cheng, A. F., Demura, H., Gaskell, R. W., Hashimoto, T., Hiraoka, K., Honda, T., and 6 co-authors. (2006) Mass and local topography measurements of Itokawa by Hayabusa. *Science* 312:5758, 1344-1349.

Adams, J. B., and McCord, T. B. (1971) Alteration of lunar optical properties: age and composition effects. *Science* 171: 567-71.

Binzel, R. P., Bus, S. J., Burbine, T. H., and Sunshine, J. M. (1996) Spectral properties of near-Earth asteroids: Evidence for sources of ordinary chondrite meteorites. *Science* 273:5277, 946-948.

Binzel, R. P., Rivkin, A. S., Stuart, J. S., Harris, A. W., Bus, S. J., and Burbine, T. H. (2004) Observed spectral properties of near-Earth objects: results for population distribution, source regions, and space weathering processes. *Icarus* 170, 259-294.

Binzel, R. P., Xu, S., and Bus, S. J. (1993) Spectral variations within the Koronis family: possible implications for the surface colors of asteroid 243 Ida. *Icarus* 106, 608-611.

Binzel, R. P., Xu, S., Bus, S. J., Skrutskie, M. F., Meyer, M., Knezek, P., and Barker, E.S. (1993b) The asteroid-meteorite connection: the discovery of a main belt ordinary chondrite asteroid. *Meteoritics* 28:3, 324.

Bottke, W. F. Jr., Cellino, A., Paolicchi, P., and Binzel, R. P. (2002) An overview of the asteroids: The Asteroids III perspective. In: Bottke, W. F. Jr., Cellino, A., Paolicchi, P., and Binzel, R. P. (Eds.), *Asteroids III.* University of Arizona Press, Tucson, pp. 3-15.

Bottke, W. F. Jr., Durda, D. D., Nesvorný, D., Jedicke, R., Morbidelli, A., Vokrouhlický, D., and Levison, H. F. (2005) Linking the collisional history of the main asteroid belt to its dynamical excitation and depletion. *Icarus* 179, 63-94.

Britt, D. T., and Consolmagno, G. J. (2001) Modeling the structure of high porosity asteroids, *Icarus* 152:1, 134-139.

Brunetto, R., Romano, F., Blanco, A., Fonti, S., Martino, M., Orofino, V., and Verrienti, C. (2006) Space weathering of silicates simulated by nanosecond pulse UV excimer laser. *Icarus* 180, 546-554.

Brunetto, R., and Strazzulla, G. (2005) Elastic collisions in ion irradiation experiments: a mechanism for space weathering of silicates. *Icarus* 179, 265-273.

Bus, S. J, and Binzel, R. P. (2002) Phase II of the Small Main-Belt Asteroid Spectroscopic Survey: a feature-based taxonomy. *Icarus* 158:1, 146-177.

Bus, S. J., Vilas, F., and Barucci, M. A. (2002) Visible-wavelength spectroscopy of asteroids. In: Bottke, W. F. Jr., Cellino, A., Paolicchi, P., and Binzel, R. P. (Eds.), *Asteroids III.* University of Arizona Press, Tuscon, pp. 169-182.

Carvano, J.M., Lazzaro, D., Mothé-Diniz, T., and Angeli, C. A. (2001) Spectroscopic survey of the Hungaria and Phocaea dynamical groups. *Icarus* 149, 173-189.

Chapman, C. R. (1996) S-type asteroids, ordinary chondrites, and space weathering: The evidence from Galileo's fly-bys of Gaspra and Ida. *Meteoritics & Planetary Science* 31, 699-725.

Chapman, C. R. (2004) Space weathering of asteroid surfaces. *Annual Review of Earth and Planetary Sciences* 32, 539-567.

Chapman, C. R., Enke, B., Merline, W. J., Nesvorný, D., Tamblyn, P., and Young, E. F. (2008) Reflectance spectra of very young asteroid families. *Asteroids, Comets, Meteors 2008*, abstract no. 8391.

Clark, B. E., Hapke, B., Pieters, C., and Britt, D. (2002) Asteroid space weathering and regolith evolution. In: Bottke, W. F. Jr., Cellino, A., Paolicchi, P., and Binzel, R. P. (Eds.), *Asteroids III.* University of Arizona Press, Tucson, pp. 585-599.

Clark, B. E., Lucey, P., Helfenstein, P., Bell, J. F. III, Peterson, C., Veverka, J., McConnochie, T., Robinson, M. S., Bussey, B., Murchie, S. L., and 2 co-authors. (2001) Space weathering on Eros: Constraints from albedo and spectral measurements of Psyche crater. *Meteoritics & Planetary Science* 36, 1617-1637.

Colonel, J., and Nash, D. (1970) Spectral reflectance and albedo of Apollo 11 lunar samples: effects of irradiation and vitrification and comparison with telescopic observations. *Geochimica et Cosmochimica Acta* Supplement 1, 2013-2024.

Doressoundiram, A., Barucci, M. A., Fulchignoni, M., and Florczak, M. (1998) Eos family: A spectroscopic study. *Icarus* 131, 15-31.

Fanale, F. P., and Clark, B. E. (1993) Chondrites, S asteroids, and space weathering: Thumping noises from the coffin? *LPSC XXIV*, Part 1, p. 463-464.

Gaffey, M. J., Bell, J. F., Brown, R. H., Burbine, T. H., Piatek, J. L., Reed, K. L., and Chaky, D. A. (1993) Spectral evidence of size dependent space weathering processes on asteroid surfaces. *LPSC XXIV*, Part 2, p. 515-516.

Gold, T. (1955) The lunar surface. *Monthly Notices of the Royal Astronomical Society* 115, 585-604.

Gradie, J., and Tedesco, E. (1982) Compositional structure of the asteroid belt. *Science* 216, 1405-1407.

Hapke, B. (2000) How to turn OCs into Ss: Space weathering in the asteroid belt. *LPSC XXXI*, abstract no. 1087.

Hapke, B. (2001) Space weathering from Mercury to the asteroid belt. *Journal of Geophysical Research* 106: E5, 10039-10073.

Hapke, B., Cassidy, W., and Wells, E. (1975) Effects of vapor-phase deposition processes on the optical, chemical and magnetic properties of the lunar regolith. *The Moon* 13, 339-353.

Hendrix, A. R., and Vilas, F. (2006) The effects of space weathering at UV wavelengths: S-class asteroids. *The Astronomical Journal* 132:3, 1396-1404.

Hendrix, A. R., Vilas, F., and Festou, M. C. (2003) Vesta's UV lightcurve: hemispheric variation in brightness and spectral reversal. *Icarus* 162, 1-9.

Hiroi, T., and Sasaki, S. (1999) Importance of olivine in S-asteroid space weathering. *LPSC XXX*, abstract no. 1444.

Hiroi, T., and Sasaki, S. (2001) Importance of space weathering simulation products in compositional modeling of asteroids: 349 Dembowska and 446 Aeternitas as examples. *Meteoritics & Planetary Science* 36, 1587-1596.

Hiroi, T., Ueda, Y., Nimura, T., Abe, M., Ishiguro, M., and Sasaki, S. (2006) A new scheme for estimating the degree of space weathering through visible multiband spectroscopy using an ECAS-type filter system such as Hayabusa Amica. *LPSC XXXVI*, abstract no. 1396.

Ishiguro, M., Hiroi, T., Tholen, D. J., Sasaki, S., Ueda, Y., Nimura, T., Abe, M., Clark, B. E., Yamamoto, A., Yoshida, F., and 9 co-authors. (2007) Global mapping of the degree of space weathering on asteroid 25143 Itokawa by Hyabusa/Amica observations. *Meteoritics & Planetary Science* 42:10, 1791-1800.

Ivezić, Ž., Lupton, R. H., Jurić, M., Tabachnik, S., Quinn, T., Gunn, J. E., Knapp, G. R., Rockosi, C. M., and Brinkmann, J. (2002) Color confirmation of asteroid families. *The Astronomical Journal 124*, 2943-2948.

Izenberg, N. R., Murchie, S. L., Bell, J. F. III, McFadden, L. A., Wellnitz, D. D., Clark, B. E., and Gaffey, M. J. (2003) Spectral properties and geologic processes on Eros from combined NEAR NIS and MSI data sets. *Meteoritics & Planetary Science 38*:7, 1053-1077

Jedicke, R., Nesvorný, D., Whiteley, R., Ivezić, Ž., and Jurić, M. (2004) An age-colour relationship for main-belt S-complex asteroids. *Nature 429*, 275-277.

Keller, L. P., and McKay, D.S. (1993) Discovery of vapor deposits in the lunar regolith. *Science 261*, 1305-1307.

Landolt, A. U. (1973) UBV photoelectric sequences in the celestial equatorial Selected Areas 92-115. *The Astronomical Journal 78*, p. 959.

Marchi, S., Paolicchi, P., Lazzarin, M., and Magrin, S. (2006) A general spectral slope-exposure relation for S-type main belt and near-Earth asteroids. *The Astronomical Journal 131*, 1138-1141.

McCord, T. B., Adams, J. B., and Johnson, T. V. (1970) Asteroid Vesta: spectral reflectivity and compositional implications. *Science 168*:3938, 1445 – 1447.

McKay, D., Fruland, R., and Heiken, G. (1974) Grain size and the evolution of lunar soils. *Geochimica et Cosmochimica Acta* Supplement 8, 3835-3957.

McKay, D., Swindle, T., and Greenberg, R. (1989) Asteroid regoliths: What we do not know. In: Binzel, R. P., Gehrels, T., and Matthews, M. (Eds), *Asteroids II*. University of Arizona Press, Tucson, pp. 617-642.

Moroz, L., Fisenko, A., Semjonova, L., Pieters, C., and Korotaeva, N. (1996) Optical effects of regolith processes on S-asteroids as simulated by laser shots on ordinary chondrite and other mafic materials. *Icarus* 122, 366-382.

Moskovitz, N. A., Jedicke, R., Gaidos, E., Willman, M., Nesvorný, D., Fevig, R., and Ivezić, Ž. (2008) The distribution of basaltic asteroids in the Main Belt. *Icarus* 198:1, 77-90.

Mothé-Diniz, T., and Nesvorný, D. (2008) Visible spectroscopy of extremely young asteroid families. *Astronomy & Astrophysics* 486, L9-L12.

Mothé-Diniz, T., Roig, F., and Carvano, J. M. (2005) Reanalysis of asteroid families structure through visible spectroscopy. *Icarus* 174, 54-80.

Nesvorný, D., Bottke, W. F., Vokrouhlický, D., Morbidelli, A., and Jedicke, R. (2005) Asteroid families. In: Lazzaro, D., Ferraz-Mello, S., and Fernández, J. A. (Eds). *Proceedings IAU Symposium* No. 229, pp. 289-299.

Nesvorný, D., Jedicke, R., Whiteley, R. J., and Ivezić, Ž. (2005b) Evidence for asteroid space weathering from the Sloan Digital Sky Survey. *Icarus* 173, 132-152.

Noble, S. K. (2005) Space weathering on asteroids. *Workshop on Oxygen in Asteroids and Meteorites*, p. 25.

Noble, S. K., Pieters, C. M., and Keller, L. P. (2004) Quantitative aspects of space weathering: Implications for regolith breccia meteorites and asteroids. *LPSC XXXV*, abstract no. 1301.

Noble, S. K., Pieters, C. M., and Keller, L. P. (2007) An experimental approach to understanding the optical effects of space weathering. *Icarus* 192, 629-642.

Pieters, C. M., Fischer, E., Rode, O., and Basu, A. (1993) Optical effects of space weathering: The role of the finest fraction. *Journal of Geophysical Research* 98, 20817-20824.

Pieters, C. M., Taylor, L., Noble, S., Keller, L., Hapke, B., Morris, R., Allen, C., McKay, D., and Wentworth, S. (2000) Space weathering on airless bodies: Resolving a mystery with lunar samples. *Meteoritics & Planetary Science* 32, 1101-1107.

Purgathofer, A. T. (1969) UBV sequences in selected star fields. *Bulletin of the Lowell Observatory* 7:10, bulletin no. 147, p. 98-111.

Rabinowitz, D. L. (1998) Size and orbit dependent trends in the reflectance colors of Earth-approaching asteroids. *Icarus* 134, 342-346.

Romanishin, W. (2006) An introduction to astronomical photometry using CCDs. Online: http://observatory.ou.edu/book2513.html.

Saito, J., Miyamoto, H., Nakamura, R., Ishiguro, M., Michikami, T., Nakamura, A. M., Demura, H., Sasaki, S., Hirata, N., Honda, C., and 24 co-authors. (2006) Detailed images of asteroid 25143 Itokawa from Hayabusa. *Science* 312:5778, 1341-1344.

Sasaki, S., and Hiroi, T. (2008) How does space weathering depend on the surface condition of airless bodies (asteroids, the Moon, and Mercury)? *LPSC XXXIX*, abstract no. 1625.

Sasaki, S., Nakamura, K., Hamabe, Y., Kurahashi, K., and Hiroi, T. (2001) Production of iron nanoparticles by laser irradiation in a simulation of lunar-like space weathering. Nature 410, 555-557.

Sasaki, S., Nimura, T., Hiroi, T., Ishiguro, M., Hirata, N., Abe, M., Ueda, Y., Yamamoto, A., and Clark, B. E. (2006). Space weathering of rock surface without regolith: laboratory simulation of spectral change. *LPSC XXXVII*, abstract no. 1705.

Sasaki, S., Ueda, Y., Kurahashi, E., Loeffler, M., and Hiroi, T. (2004) Change of asteroid reflectance spectra by space weathering: pulse laser irradiation on meteorite samples. *LPSC XXXV*, abstract no. 1538.

Scott, E. R. D. (2002) Meteorite evidence for the accretion and collisional evolution of asteroids. In: Bottke, W. F. Jr., Cellino, A., Paolicchi, P., and Binzel, R. P. (Eds.), *Asteroids III*. University of Arizona Press, Tucson, pp. 697-710.

Slivan, S., and Binzel, R. P. (1996) Forty-eight new rotation lightcurves of 12 Koronis family asteroids. *Icarus* 124, 452-470.

Strazzulla, G., Dotto, E., Binzel, R., Brunetto, R., Barucci, M. A., Blanco, A., and Orofino, V. (2005) Spectral alteration of the meteorite Epinal (H5) induced by heavy ion irradiation: a simulation of space weathering effects on near-Earth asteroids. *Icarus* 174, 31-35.

Tedesco, E. F., Tholen, D. J., and Zellner, B. (1982) The eight-color asteroid survey: Standard stars. *The Astronomical Journal* 87:11, 1585-1592.

Tholen, D. J. (1984) Asteroid taxonomy from cluster analysis of Photometry. PhD Thesis, University of Arizona, Tucson.

Ueda, Y., Hiroi, T., Sasaki, S., and Miyamoto, M. (2005) Evidence of enhanced space weathering effect by coexisting metallic iron. *Meteoritics & Planetary Science* 40, 5198.

Veverka, J., Helfenstein, P., Lee, P., Thomas, P., McEwen, A., Belton, M., Klaasen, K., Johnson, T. V., Granahan, J., Fanale, F., and 2 co-authors. (1996) Ida and Dactyl: Spectral Reflections and Color variations. *Icarus* 120, 66-76.

Warner, B. D. (2006) *A Practical Guide to Lightcurve Photometry and Analysis*. Springer, New York, pp. 23-24.

Willman, M., Jedicke, R., Nesvorný, D., Moskovitz, N., Ivezić, Ž., and Fevig, R. (2008) Redetermination of the space weathering rate using spectra of Iannini asteroid family members. *Icarus* 195, 663-673.

Yamada, M., Sasaki, S., Fujiwara, A., Hiroi, T., Hasegawa, S., Nagahara, H., Ohashi, H., Otake, H., and Yano, H. (1999) Simulation of space weathering by nanosecond pulse laser heating and proton implantation: difference of olivine and pyroxene samples. *LPSC XXX*, abstract no. 1566.

Zellner, B., Thirunagari, A., and Bender, D. (1985) The large-scale structure of the asteroid belt. *Icarus* 62, 505-511.

Zellner, B., Tholen, D. J., and Tedesco, E. F. (1985b) The eight-color asteroid survey: Results for 589 minor planets. *Icarus* 61, 355-416.